Stomach Curvature is Generated by Left-right Asymmetric Gut Morphogenesis

Adam Davis[1†‡], Nirav M. Amin[1‡], Caroline Johnson[1], Kristen Bagley[1], H. Troy Ghashghaei[1], Nanette Nascone-Yoder[1*]

[1] Department of Molecular Biomedical Sciences, College of Veterinary Medicine, North Carolina State University, Raleigh, NC 27607.
[†] Current: Department of Biology and Physical Sciences, Gordon State College, Barnesville, GA 30204.
‡ These authors contributed equally to this work.
* Correspondence to: nmnascon@ncsu.edu

Key Words: Left-right, asymmetry, stomach, gut, morphogenesis, *Pitx2*

Summary Statement: Left-right patterning creates morphogenetic differences between the left and right walls of the vertebrate foregut that generate the asymmetric curvature of the stomach.

Abstract:

Left-right (LR) asymmetry is a fundamental feature of internal anatomy, yet the emergence of morphological asymmetry remains one of the least understood phases of organogenesis. Asymmetric rotation of the intestine is directed by forces outside of the gut, but the morphogenetic events that generate anatomical asymmetry in other regions of the digestive tract remain unknown. Here we show that the mechanisms that drive the curvature of the stomach are intrinsic to the gut tube itself. The left wall of the primitive stomach expands more than the right wall, as the left epithelium becomes more polarized and undergoes radial rearrangement. These asymmetries exist across species, and are dependent on LR patterning genes, including *FoxJ1*, *Nodal* and *Pitx2*. Our findings have implications for how LR patterning manifests distinct types of morphological asymmetries in different contexts.

Introduction:

The external symmetry of bilateria belies the marked left-right (LR) asymmetry of their internal organs. In vertebrates, the LR axis is established by nodal cilia, which activate expression of the TGF-β molecule, *Nodal*, exclusively on the embryo's left side (Levin et al., 1995; Lowe et al., 1996; Murcia et al., 2000; Okada et al., 1999). Downstream of *Nodal*, the transcription factor *Pitx2c* is then expressed along the left side of developing organs as they acquire morphological asymmetry (Campione et al., 1999). These patterning events culminate in anatomical laterality, including left- or right-side organ position, LR asymmetry in the shapes/sizes of paired organs, or intrinsic morphological disparity between the sides of an individual organ (Capdevila et al., 2000).

The J-shaped curvature of the stomach is an archetype of such laterality. The exact configuration of this organ varies among species with different diets, yet its distinctive shape, characterized by a longer "greater curvature" on the left, and shorter "lesser curvature" on the right, is highly conserved and integral to normal function (Stevens and Hume, 2004). Early embryologists contended that stomach anatomy results from a developmental rotation in which the ostensibly enlarged dorsal surface turns leftward to become the greater curvature (Liebermann-Meffert, 1969). However, some have argued that rotation is illusory and that curvature emerges via an intrinsic process, e.g., asymmetric growth (Kanagasuntheram, 1957; Liebermann-Meffert, 1969). Remarkably, the cellular and molecular events that drive stomach curvature have never been experimentally addressed.

Results and Discussion:

Stomach asymmetry is independent of rotation

We compared stomach curvature formation in two animal models, the mouse and the frog (*Xenopus laevis*). In both species, the slit-like lumen of the still-straight primitive stomach [mouse stage E10 and frog stage 34 (Nieuwkoop and Faber, 1994)] is initially aligned with the dorsal-ventral (DV) axis of the embryo (Fig. 1C, E). If the dorsal face of the organ rotates leftward during development, we would expect its DV axis to shift clockwise with respect to the embryonic midline as asymmetric morphology emerges (in posterior view, Fig. 1A). Surprisingly, we find no indication of such a shift in either species. However, in both the mouse (Fig. 1C-D) and frog (Fig. 1E-F), the left wall of the early stomach becomes longer than the right wall and begins to bend outward, skewing the nascent lumen leftward. These LR differences are also evident in orthogonal planes of section (not shown), indicating

that a general expansion of the left wall occurs concomitantly with the emergence of overt laterality. This intrinsic asymmetry is evident prior to mesogastrial remodeling; indeed, in the frog, a mesogastrium is not detectable when stomach asymmetry becomes obvious. Thus, external tissues/forces may not be required for stomach curvature. These observations are congruent with a model of asymmetric stomach morphogenesis driven by preferential expansion of the left wall (i.e., Fig. 1B).

Differential tissue architecture develops in the left and right stomach walls

To define the morphogenetic events that drive asymmetric expansion, we compared contralateral tissue architecture during stomach development (Fig. 2). The walls of the gut tube are comprised of an inner layer of endoderm which will become the epithelium, and an outer layer of mesoderm, which will become visceral muscle and connective tissue. Although the relative thickness of each layer varies between mouse and frog embryos, the tissues of the left stomach wall become significantly thinner than the right wall at stages preceding and coinciding with curvature in both species (Figs. 2A-B, E-F, I-J and M-N).

In vertebrates, the transcription factor *FoxJ1* is a master regulator of motile ciliogenesis required for proper establishment of the LR axis (Brody et al., 2000; Chen et al., 1998; Stubbs et al., 2008; Tamakoshi et al., 2006; Walentek et al., 2012). To determine whether the differential morphogenesis of the stomach walls is dependent on LR patterning, we analyzed *FoxJ1* mutant mouse embryos. In *FoxJ1* heterozygotes, which have normal LR patterning (Muthusamy et al., 2014), the preferential lengthening of the left stomach wall and asymmetric lumen expansion proceed normally (Fig. 2B). However, in *FoxJ1* homozygous null embryos, in which nodal cilia are defective and LR patterning and organ morphology is consequently randomized, the length of the opposing stomach walls is equivalent and the stomach appears straightened (Fig. 2C-D; Fig. S1). Moreover, there is no LR asymmetry in the thickness of the tissue layers (Fig. 2G-H).

LR asymmetry is propagated by the expression of *nodal* on the left side of the embryo (Levin et al., 1995; Lowe et al., 1996; Murcia et al., 2000; Okada et al., 1999). *Xenopus* neurulae exposed to a small molecule inhibitor of the Nodal receptor (e.g., SB505124; Fig. S2A-B) have decreased Nodal signaling, perturbed laterality and aberrant organogenesis (Dush et al., 2011). In such embryos, the lengths of the contralateral stomach walls are equal (Fig. S2C), and the leftward curvature of the stomach is eliminated (Fig. 2K-L; 56%; n=38; Fig. S2D). Furthermore, there is no difference in endoderm/mesoderm thickness (Fig. 2O-P). Thus, the early morphological differences between the sides of the stomach are a

manifestation of LR patterning events.

Stomach curvature is accompanied by left-right asymmetric epithelial morphogenesis

As radial rearrangement of the endoderm thins and expands other regions of the gut tube (Chalmers and Slack, 2000; Reed et al., 2009), we compared the number of endoderm cell layers within the left and right stomach walls. Prior to curvature, there are no LR differences (L/R ratio ~ 1). However, as curvature emerges, fewer layers are apparent in the left wall (L/R ratio<1; average mouse = 0.44, $p< 0.01$; frog = 0.77, $p< 0.01$; Fig. 2Q-T). Since the total number and shape of cells on each side remains equivalent during curvature (Fig. S3A-C), these results indicate that preferential expansion of the left wall is driven by LR asymmetric cell rearrangement.

Appearing concomitantly with LR differences in cell rearrangement are asymmetries in endoderm cell polarity. This is not surprising as polarity is a prerequisite for cells to undergo radial rearrangement (Marsden and Desimone, 2001), and endoderm cells acquire apicobasal polarity as they rearrange to lengthen the intestine and form the mature digestive epithelium (Grosse et al., 2011; Matsumoto et al., 2002; Reed et al., 2009). In *FoxJ1* heterozygous mice, the endoderm of the posterior right stomach wall becomes irregularly stratified, while the left endoderm is highly polarized (as indicated by apical enrichment of tubulin; Fig. 3A, D, G). This LR asymmetric tissue architecture is variably perturbed in heterotaxic *FoxJ1*$^{-/-}$ embryos, consistent with the randomization of LR patterning cues (Zhang et al., 2004). In one *FoxJ1*$^{-/-}$ embryo, both left and right walls of the straightened stomach are highly polarized (Fig. 3B, E, H), and the number of endoderm cell layers remains equivalent (average L/R ratio = 1.19, $p< 0.01$; Fig. 2Q-R) while, in another case, both sides exhibit irregular architecture (Fig. 3C, F, I).

In frogs, the endoderm is substantially thicker than in the mouse; nonetheless, similar LR differences appear as the left endoderm adopts a more polarized morphology (Fig. 3J, L, N; Fig. S4A, B, E, H). Interestingly, in the straightened stomachs of Nodal-deficient (i.e., SB505124-treated) embryos, the left endoderm closely resembles the normal right side (Fig. 3K, M, O) and the number of cell layers remains equivalent (average L/R ratio =1.16, $p< 0.01$; Fig. 2S-T). Thus, in both species, the emergence of morphological stomach laterality correlates with LR asymmetries in endoderm polarity and rearrangement.

Pitx2 controls left stomach epithelial morphogenesis

The expression of *Pitx2c* is limited to the left wall during stomach development (Liu et al., 2001; Logan et al., 1998), and is required for normal organ laterality (Bamforth et al., 2004; Campione et al., 1999; Liu et al., 2001; Logan et al., 1998; Ryan et al., 1998). *Pitx2c* null mice may exhibit reversed or midline stomach orientations (Bamforth et al., 2004), although the mechanism by which Pitx2 impacts stomach morphogenesis is unknown. In other regions of the digestive tract, *Pitx* isoforms are associated with polarized epithelial morphogenesis and tissue expansion (e.g., intestine lengthening, cecal budding) (Al et al., 2012; Campione et al., 1999; Chung et al., 2011). Thus, asymmetric expression of *Pitx2c* in left stomach may drive the observed asymmetries in endoderm morphogenesis.

Consistent with this hypothesis, CRISPR-Cas9 mediated mutation of *Xenopus pitx2c* results in straightened stomachs in which the left wall does not lengthen or thin, and exhibits abnormal epithelial architecture (Fig. S5) and failed cell rearrangement [as indicated by an increased number of cell layers in the left epithelium (average L/R ratio =1.31, $p< 0.05$)], confirming that *pitx2c* is specifically required for key aspects of asymmetric stomach morphogenesis. However, as CRISPR-Cas9 editing introduces random mutations (Fig S5E), it is impossible to spatially define the exact cells harboring null mutations and the extent to which Pitx2 activity is altered in each F0 animal. Therefore, to specifically determine the role of *pitx2c* within left stomach, we also capitalized on the amenability of *Xenopus* for targeting gain- or loss-of-function reagents specifically to the left or right side of developing organs by microinjection, a strategy not easily feasible in mouse (Blum et al., 2009; Duncan and Khokha, 2016).

First, we employed two independent morpholino oligonucleotides (MO) to deplete Pitx2c translation in a targeted manner (see Fig. S6A-B). When *pitx2c* MO is microinjected to target the right stomach, stomach curvature is unaffected (8%; n=37); however, if *pitx2c* MO is targeted to the left side, the organ fails to curve [41% reduced/absent greater curvature (n=37), compared to control MO, 4% (n=41)], recapitulating the CRISPR-Cas9 phenotype (Fig. 4A-B; Fig S6C). Concomitant with lack of curvature, the Pitx2c-deficient left epithelium now resembles the less organized and unpolarized right epithelium (Fig. 4E-F, I-J, M-N, Q-R; Fig. S4C, F, I). The *pitx2c*-MO-injected left wall does not thin (Fig. S6D-E), nor do the endoderm cells rearrange, as indicated by increased cell layers on the left (Fig. S6F; average L/R ratio control MO =0.83; *pitx2c*-MO = 1.34). Interestingly, the endoderm and mesoderm layers of the stomach wall may influence each other during asymmetric morphogenesis, as MO-injected clones limited primarily to the endoderm or mesoderm layer

also perturb the architecture of neighboring, uninjected tissue (Fig. S7). This reciprocal influence is well-established in foregut patterning (Womble et al., 2016).

To determine whether *pitx2c* alone is sufficient to impart apicobasal polarity to the endoderm, we targeted mRNA encoding a glucocorticoid-inducible version of Pitx2c, *pitx2c-GR* (Chung et al., 2011), to the right stomach. Induction of ectopic Pitx2c activity by dexamethasone eliminates stomach curvature (60%, n=82; Fig. 4C-D), while un-induced control stomachs remain unaffected (10%; n=90). Strikingly, inducing Pitx2c-GR results in ectopic polarization of the right endoderm, with the affected tissue expanding into the stomach lumen (Fig. 4G-H, K-L) and expressing higher levels of polarity markers compared to adjacent un-induced tissue (Fig. 4O-P, S-T; Fig. S4D, G, J). Thus, *pitx2c* is necessary and sufficient to promote epithelial polarization in stomach endoderm.

How anatomical asymmetries are generated is relevant to the origin of novelty during evolution and integral to the etiology of birth defects but, for most organs, this critical phase of organogenesis is poorly understood. Recent work suggests asymmetrical intestinal rotation is generated by LR differences in the dorsal mesentery that connects the midgut to the body wall—not in the gut tube itself, which remains symmetrical during the rotation process (Davis et al., 2008; Kurpios et al., 2008; Welsh et al., 2013). In contrast, our results indicate that stomach curvature is driven by asymmetric morphogenesis within the organ itself.

Moreover, while *Pitx2c* elicits tissue condensation in left dorsal mesentery (Davis et al., 2008), *Pitx2c* elicits tissue expansion in left stomach, suggesting that the final manifestation of *Pitx2c* activity in different organs is not universal, but influenced by geometric context (e.g., internal or external to the gut tube) and tissue type. Our study suggests that the final topology of the digestive tract is the end-product of at least two Pitx2-mediated symmetry-breaking processes: mesentery distortion, which positions the gut tube asymmetrically in the body cavity, and asymmetric gut morphogenesis, which sculpts disparate morphologies within the contralateral walls of the gut itself.

Materials and Methods

Animals and Genotyping

Animals used in accordance with NCSU IACUC regulations. *Xenopus in vitro* fertilization, embryo culture and staging were as described (Nieuwkoop and Faber, 1994; Sive et al., 1998). Heterozygous *FoxJ1*$^{+/creERT2}$ mice (Muthusamy et al., 2014) were used in timed pregnancy matings to obtain *FoxJ1*$^{+/creERT2}$ (i.e., *FoxJ1*$^{+/-}$) and *FoxJ1*$^{creERT2/creERT2}$ (i.e., *FoxJ1*$^{-/-}$) embryos. Noon on day of vaginal plug discovery was defined as E0.5. Embryos were harvested in ice-cold 0.1M phosphate buffered saline (PBS) and fixed overnight in 4% paraformaldehyde in PBS. PCR was used to identify homozygous *creERT2* insertion into *FoxJ1* locus (Muthusamy et al., 2014); see Supplementary Materials and Methods for genotyping primers.

Xenopus Loss- and Gain-of-function experiments

Pharmacological (e.g., SB505124) dosing of *Xenopus* neurulae (stage 19/20) was conducted as described (Dush et al., 2011). SB505124 was diluted to 5 μM in culture medium (0.1X MMR); an equal volume of DMSO (solvent) was used as control.

Microinjection was performed at 1-cell (CRISPR) or 8-cell stages (morpholinos and mRNA), using established methods (Sive et al., 1998). Co-injected GFP mRNA validated tissue targeting. *Pitx2*-GR mRNA injected embryos were exposed to dexamethasone (10 μM) or ethanol (control) from stage 19/20. Synthetic mRNA was transcribed *in vitro* (mMessage mMachine kit; ThermoFisher). Cas9 mRNA and gRNAs were synthesized as described (Guo et al., 2014). See Supplementary Materials and Methods for morpholino/gRNA sequences and mutation analyses.

Embryos were cultured through stage 34, 37, 39 or 42 and collected for phenotyping/immunofluorescence.

Immunofluorescence

Tissue processing, sectioning and immunostaining was as described (Dush and Nascone-Yoder, 2013). See Supplementary Materials and Methods for antibodies. Mouse sections in Figure 1 were downloaded from the EMAP eMouse Atlas Project (http://www.emouseatlas.org) (Richardson et al., 2014).

Methodology and Statistics

All experiments were performed at least in triplicate, with similar results. Morphometric measurements performed with Image J, Photoshop or eMouse measuring tools, EMAP eMouse Atlas Project (http://www.emouseatlas.org). Statistical significance determined by ANOVA with post-hoc Tukey HSD; see Supplementary Materials and Methods for details.

Acknowledgments:

We thank N. Muthasamy for assistance with mouse genotyping.

Author contributions:

A.D., N.M.A., C.J. and K.B. performed experiments; N.N-Y. conceived of project and wrote manuscript; H.T.G. provided mouse strains.

Funding: This work was supported by the National Institutes of Health [R01DK085300 and R21OD017963 to N.N-Y., R01NS062182 to H.T.G, T32ES007046 to A.D.]

References

Al, A. D., Sala, F. G., Baptista, S., Galzote, R., Danopoulos, S., Tiozzo, C., Gage, P., Grikscheit, T., Warburton, D., Frey, M. R. et al. (2012). FGF9-Pitx2-FGF10 signaling controls cecal formation in mice. *Dev. Biol.* **369,** 340-348.

Bamforth, S. D., Braganca, J., Farthing, C. R., Schneider, J. E., Broadbent, C., Michell, A. C., Clarke, K., Neubauer, S., Norris, D., Brown, N. A. et al. (2004). Cited2 controls left-right patterning and heart development through a Nodal-Pitx2c pathway. *Nat. Genet.* **36,** 1189-1196.

Blum, M., Beyer, T., Weber, T., Vick, P., Andre, P., Bitzer, E. and Schweickert, A. (2009). Xenopus, an ideal model system to study vertebrate left-right asymmetry. *Dev. Dyn.* **238,** 1215-1225.

Blum, M., Feistel, K., Thumberger, T. and Schweickert, A. (2014). The evolution and conservation of left-right patterning mechanisms. *Development.* **141,** 1603-1613.

Brody, S. L., Yan, X. H., Wuerffel, M. K., Song, S. K. and Shapiro, S. D. (2000). Ciliogenesis and left-right axis defects in forkhead factor HFH-4-null mice. *Am. J. Respir. Cell Mol. Biol.* **23,** 45-51.

Campione, M., Steinbeisser, H., Schweickert, A., Deissler, K., van Bebber, F., Lowe, L. A., Nowotschin, S., Viebahn, C., Haffter, P., Kuehn, M. R. et al. (1999). The homeobox gene Pitx2: mediator of asymmetric left-right signaling in vertebrate heart and gut looping. *Development* **126,** 1225-1234.

Capdevila, J., Vogan, K. J., Tabin, C. J. and Izpisua Belmonte, J. C. (2000). Mechanisms of left-right determination in vertebrates. *Cell* **101,** 9-21.

Chalmers, A. D. and Slack, J. M. (2000). The *Xenopus* tadpole gut: fate maps and morphogenetic movements. *Development* **127,** 381-392.

Chen, J., Knowles, H. J., Hebert, J. L. and Hackett, B. P. (1998). Mutation of the mouse hepatocyte nuclear factor/forkhead homologue 4 gene results in an absence of cilia and random left-right asymmetry. *J. Clin. Invest.* **102,** 1077-1082.

Chung, M., Nascone-Yoder, N., Drysdale, T. and Wallingford, J. B. (2011). Direct activation of Shroom3 transcription by Pitx proteins drives epithelial morphogenesis in the developing gut. *Development* **137,** 1339-1349.

Davis, N. M., Kurpios, N. A., Sun, X., Gros, J., Martin, J. F. and Tabin, C. J. (2008). The chirality of gut rotation derives from left-right asymmetric changes in the architecture of the dorsal mesentery. *Dev Cell* **15,** 134-145.

Duncan, A. R. and Khokha, M. K. (2016). Xenopus as a model organism for birth defects-Congenital heart disease and heterotaxy. *Semin. Cell Dev. Biol.* **51,** 73-79.

Dush, M., McIver, A., Parr, M., Young, D., Fisher, J., Newman, D., Hauck, M., Deiters, A. and Nascone-Yoder, N. (2011). Heterotaxin: a novel TGF-β signaling inhibitor identified in a multi-phenotype profiling screen in *Xenopus* embryos. *Chemistry and Biology* **18,** 252-263.

Dush, M. K. and Nascone-Yoder, N. M. (2013). Jun N-terminal kinase maintains tissue integrity during cell rearrangement in the gut. *Development* **140,** 1457-1466.

Grosse, A. S., Pressprich, M. F., Curley, L. B., Hamilton, K. L., Margolis, B., Hildebrand, J. D. and Gumucio, D. L. (2011). Cell dynamics in fetal intestinal epithelium: implications for intestinal growth and morphogenesis. *Development* **138,** 4423-4432.

Kanagasuntheram, R. (1957). Development of the human lesser sac. *J. Anat.* **91,** 188-206.

Kurpios, N. A., Ibanes, M., Davis, N. M., Lui, W., Katz, T., Martin, J. F., Belmonte, J. C. and Tabin, C. J. (2008). The direction of gut looping is established by changes in the extracellular matrix and in cell:cell adhesion. *Proc Natl Acad Sci U S A* **105,** 8499-8506.

Levin, M., Johnson, R. L., Stern, C. D., Kuehn, M. and Tabin, C. (1995). A molecular pathway determining left-right asymmetry in chick embryogenesis. *Cell* **82,** 803-814.

Liebermann-Meffert, D. (1969). [Development of form and position of the human stomach and its mesenteries]. *Acta Anat. (Basel.)* **72,** 376-410.

Liu, C., Liu, W., Lu, M. F., Brown, N. A. and Martin, J. F. (2001). Regulation of left-right asymmetry by thresholds of Pitx2c activity. *Development* **128,** 2039-2048.

Logan, M., Pagan-Westphal, S. M., Smith, D. M., Paganessi, L. and Tabin, C. J. (1998). The transcription factor Pitx2 mediates situs-specific morphogenesis in response to left-right asymmetric signals. *Cell* **94,** 307-317.

Lowe, L. A., Supp, D. M., Sampath, K., Yokoyama, T., Wright, C. V., Potter, S. S., Overbeek, P. and Kuehn, M. R. (1996). Conserved left-right asymmetry of nodal expression and alterations in murine situs inversus. *Nature* **381,** 158-161.

Marsden, M. and Desimone, D. W. (2001). Regulation of cell polarity, radial intercalation and epiboly in Xenopus: novel roles for integrin and fibronectin. *Development* **128,** 3635-3647.

Matsumoto, A., Hashimoto, K., Yoshioka, T. and Otani, H. (2002). Occlusion and subsequent re-canalization in early duodenal development of human embryos: integrated organogenesis and histogenesis through a possible epithelial-mesenchymal interaction. *Anat. Embryol. (Berl)* **205,** 53-65.

Murcia, N. S., Richards, W. G., Yoder, B. K., Mucenski, M. L., Dunlap, J. R. and Woychik, R. P. (2000). The Oak Ridge Polycystic Kidney (orpk) disease gene is required for left-right axis determination. *Development.* **127,** 2347-2355.

Muthusamy, N., Vijayakumar, A., Cheng, G., Jr. and Ghashghaei, H. T. (2014). A knock-in Foxj1(CreERT2::GFP) mouse for recombination in epithelial cells with motile cilia. *Genesis.* **52,** 350-358.

Nieuwkoop,P.D. and Faber,J. (1994). *Normal Table of Xenopus laevis (Daudin)*. New York: Garland Publishing Inc.

Okada, Y., Nonaka, S., Tanaka, Y., Saijoh, Y., Hamada, H. and Hirokawa, N. (1999). Abnormal nodal flow precedes situs inversus in iv and inv mice. *Mol. Cell* **4,** 459-468.

Reed, R., Womble, M., Dush, M., Tull, R., Bloom, S., Morckel, A., Devlin, E. and Nascone-Yoder, N. (2009). The morphogenesis of the primitive gut tube is generated by Rho/ROCK/Myosin II-mediated endoderm rearrangements. *Dev. Dyn.* **238,** 3111-3125.

Richardson, L., Venkataraman, S., Stevenson, P., Yang, Y., Moss, J., Graham, L., Burton, N., Hill, B., Rao, J., Baldock, R. A. et al. (2014). EMAGE mouse embryo spatial gene expression database: 2014 update. *Nucleic Acids Res.* **42,** D835-D844.

Ryan, A. K., Blumberg, B., Rodriguez-Esteban, C., Yonei-Tamura, S., Tamura, K., Tsukui, T., de la, P. J., Sabbagh, W., Greenwald, J., Choe, S. et al. (1998). Pitx2 determines left-right asymmetry of internal organs in vertebrates. *Nature* **394,** 545-551.

Sive,H.L., Grainger,R.M., and Harland,R.M. (1998). *Early Development of Xenopus laevis*. Cold Spring Harbor, New York: Cold Spring Harbor Laboratory Press.

Stevens,C.E. and Hume,I.D. (2004). *Comparative Physiology of the Vertebrate Digestive System*. Cambridge: Cambridge University Press.

Stubbs, J. L., Oishi, I., Izpisua Belmonte, J. C. and Kintner, C. (2008). The forkhead protein Foxj1 specifies node-like cilia in Xenopus and zebrafish embryos. *Nat. Genet.* **40,** 1454-1460.

Tamakoshi, T., Itakura, T., Chandra, A., Uezato, T., Yang, Z., Xue, X. D., Wang, B., Hackett, B. P., Yokoyama, T. and Miura, N. (2006). Roles of the Foxj1 and Inv genes in the left-right determination of internal organs in mice. *Biochem. Biophys. Res. Commun.* **339,** 932-938.

Walentek, P., Beyer, T., Thumberger, T., Schweickert, A. and Blum, M. (2012). ATP4a is required for Wnt-dependent Foxj1 expression and leftward flow in Xenopus left-right development. *Cell Rep.* **1,** 516-527.

Welsh, I. C., Thomsen, M., Gludish, D. W., Alfonso-Parra, C., Bai, Y., Martin, J. F. and Kurpios, N. A. (2013). Integration of Left-Right Pitx2 Transcription and Wnt Signaling Drives Asymmetric Gut Morphogenesis via Daam2. *Dev. Cell* **26,** 629-644.

Womble, M., Pickett, M. and Nascone-Yoder, N. (2016). Frogs as integrative models for understanding digestive organ development and evolution. *Semin. Cell Dev. Biol.* **51,** 92-105.

Zhang, M., Bolfing, M. F., Knowles, H. J., Karnes, H. and Hackett, B. P. (2004). Foxj1 regulates asymmetric gene expression during left-right axis patterning in mice. *Biochem. Biophys. Res. Commun.* **324,** 1413-1420.

Figures

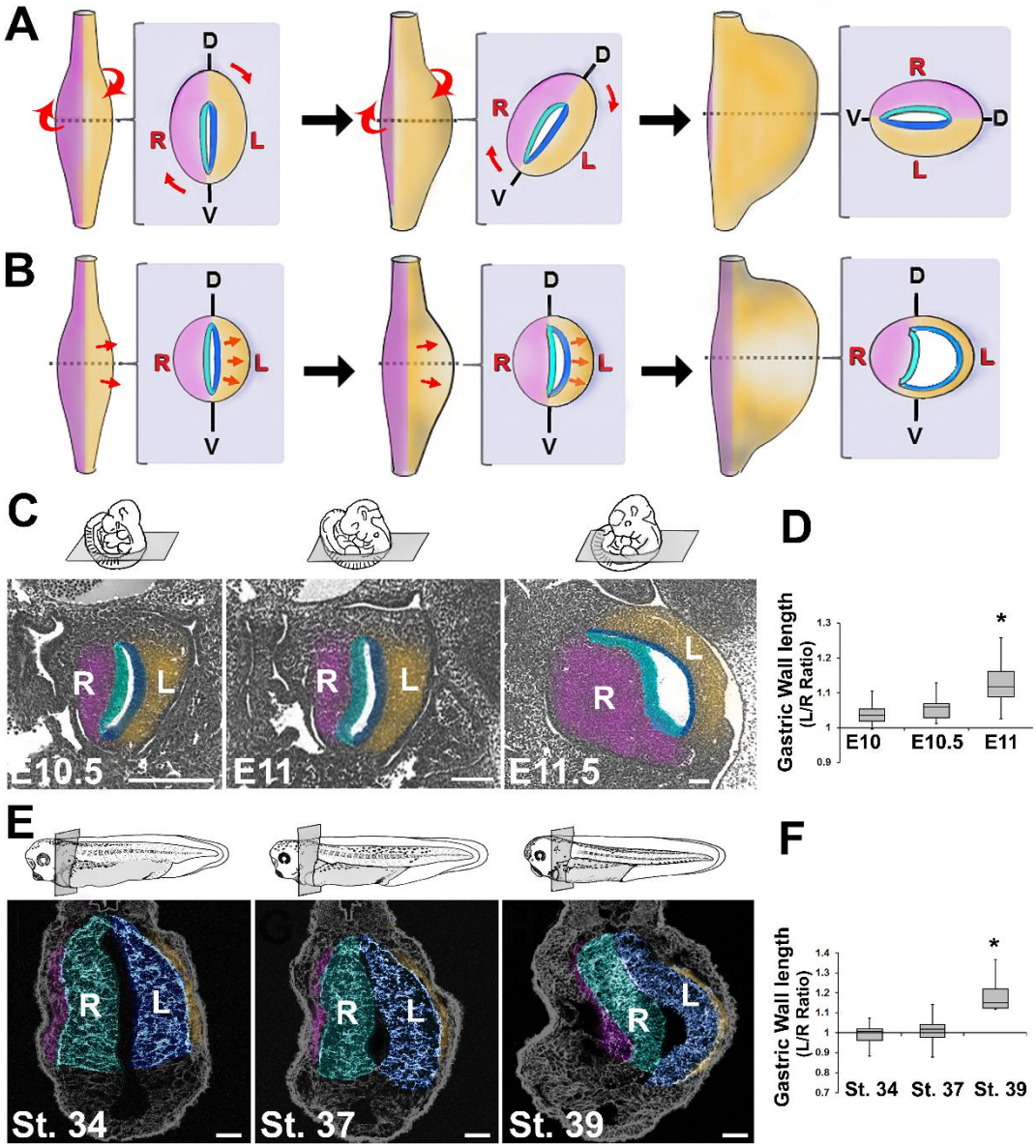

Figure 1. Early stomach undergoes leftward expansion. The rotation model (**A**) posits that the embryonic stomach (shown in ventral and posterior cross-sections at successive stages) rotates around its longitudinal axis, shifting its dorsal face leftward. An alternative model (**B**) theorizes that the left wall expands more than the right. Sections of E10.5, E11 and E11.5 mouse embryos (**C**) or St. 34, 37 and 39 frog embryos (**E**) reveal the leftward expansion of the early stomach. The left/right ratio of the lengths of the stomach walls becomes significantly greater than 1 in mouse by E11 (**D**) and in frog by Stage 39 (**F**); * denotes $p<0.05$. Sections in **C** and **E** are false-colored to match diagrams in **A** and **B**, highlighting layers of the stomach: right mesoderm, pink; right endoderm, teal; left endoderm, blue; left mesoderm, gold. In all sections, dorsal is up and left side of animal is on right side of image. Dorsal, D; ventral, V; left, L; right, R. Scalebars in **C**, 500 μM (E11.5, 150 μM); **E**, 75 μM.

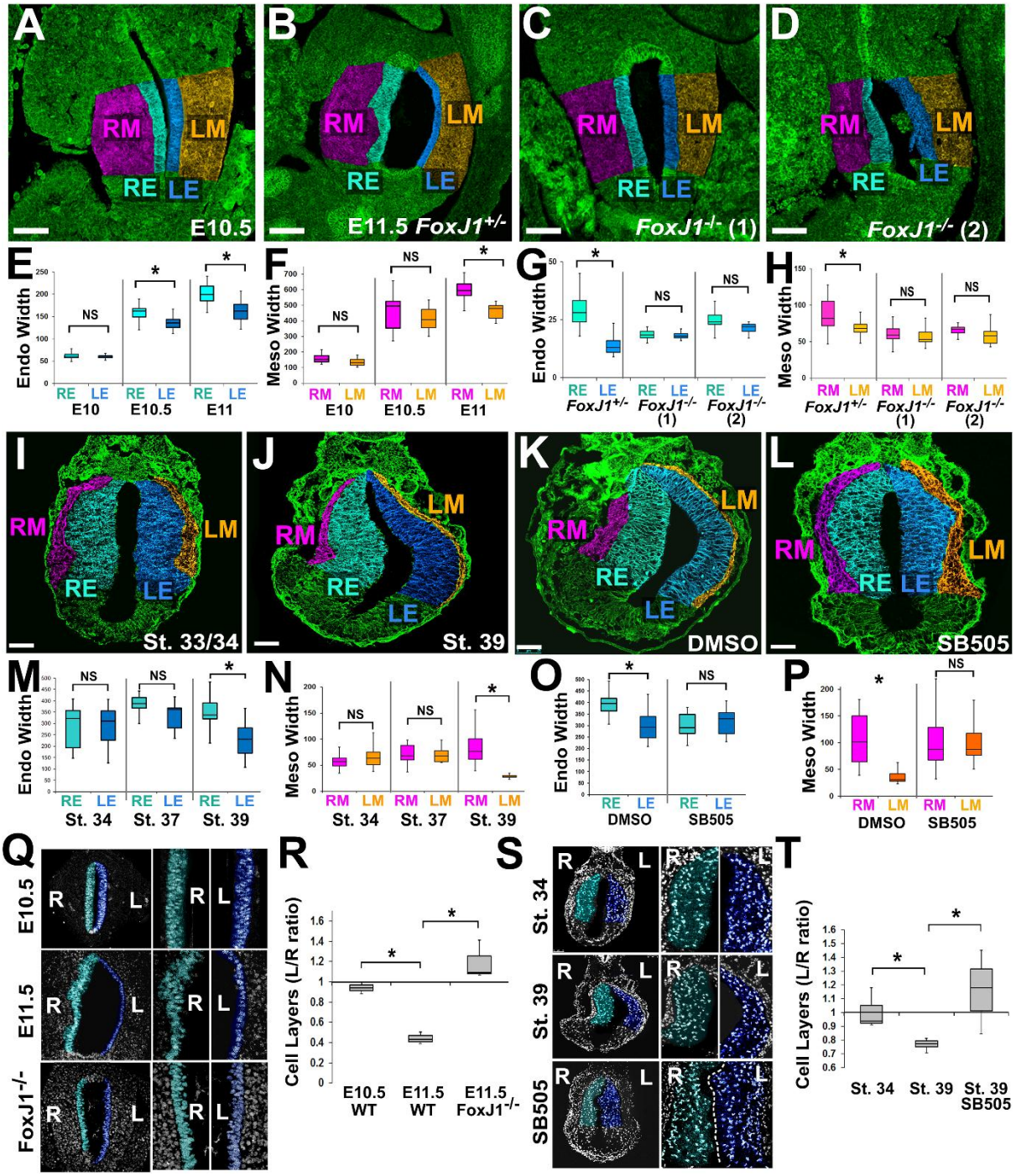

Figure 2. Asymmetries in tissue architecture are regulated by left-right patterning. Sections through mouse (**A-D**) or frog (**I-L**) stomachs were stained for β-catenin or integrin (green), respectively, and false color-coded as in Figure 1 (RE, right endoderm; LE, left endoderm; RM, right mesoderm; LM, left mesoderm). The widths of the endoderm (Endo) and mesoderm (Meso) are significantly different by E10.5-11 in mouse (**E, F**) and St. 39 in frog (**M, N**). In *FoxJ1*$^{+/-}$ controls (E11.5), the lumen expands leftward and left-right differences in tissue width are evident (**B**); however, in *FoxJ1*$^{-/-}$ mutants, the normal leftward expansion of the stomach is perturbed (**C-D**), and left-right differences in tissue width are eliminated (**G-H**). Likewise, frog embryos exposed to DMSO show normal leftward

expansion of the stomach lumen (**K**); this is eliminated in embryos exposed to a Nodal inhibitor (SB505124; **L**), as are normal left-right differences in widths of endoderm and mesoderm (**O-P**). Nuclear staining reveals asymmetry in the number of endoderm cell layers in the right (teal) versus left (blue) stomach walls by E11.5 in mouse (**Q, R**) and St. 39 in frog (**S,T**); this asymmetry is perturbed in *FoxJ1*$^{-/-}$ mutants (**Q, R**) and in frog embryos exposed to SB505124 (**S, T**). Scalebars in **A-D**, 100 μM; **I-L**, 75 μM. * denotes $p<0.01$; NS, not significant.

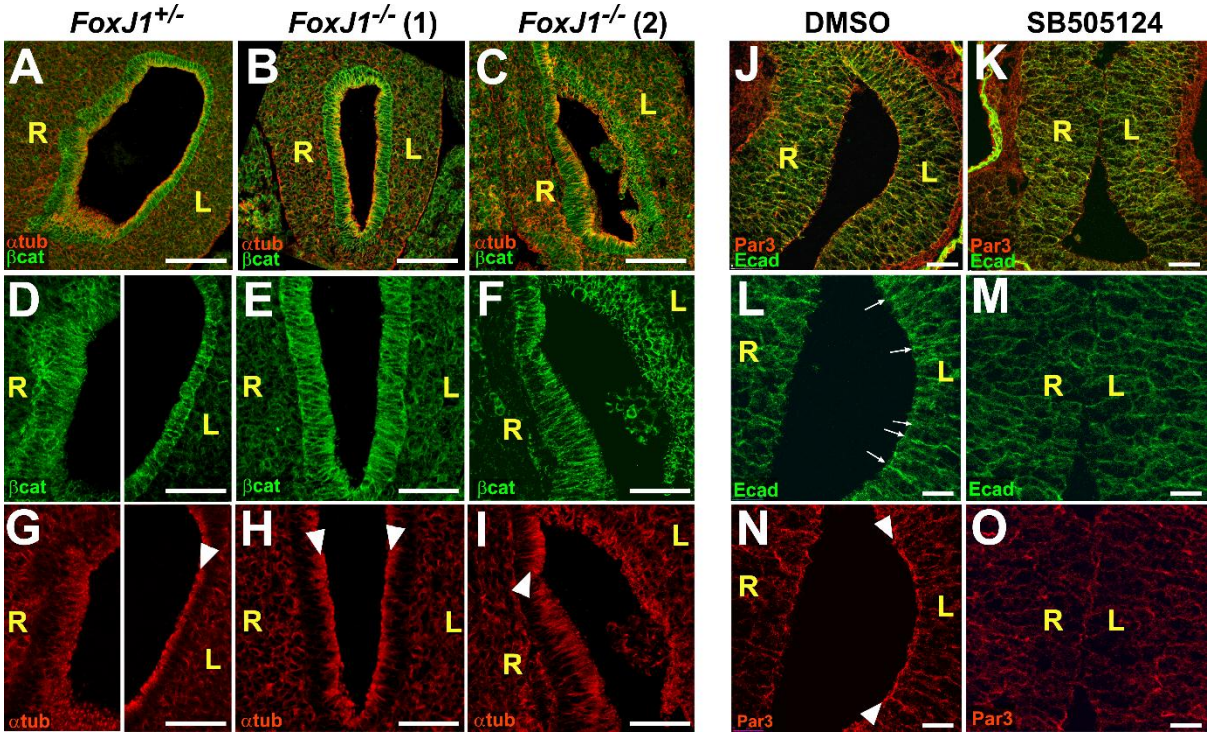

Figure 3. Asymmetries in stomach epithelial polarity are regulated by left-right signaling. Stomach sections immunostained for α-tubulin (αtub, red) and β-catenin (β-cat, green) in the E11.5 mouse (**A-I**), or Par3 (red) and E-cadherin (Ecad, green) in the St. 39 frog (**J-O**), reveal left-right differences in endoderm morphogenesis. In the posterior stomach of *FoxJ1*$^{+/-}$ mice, right endoderm is irregular, while left endoderm is more organized (**D**) and highly polarized, as indicated by tight apical concentration of α–tubulin (αtub, red; arrowhead, **G**). Both walls of *FoxJ1*$^{-/-}$ mutant embryo [*FoxJ1*$^{-/-}$(1), **B, E, H**], are comprised of polarized cells with tight apical concentration of αtub (arrowheads, **H**); both sides resemble control left epithelium. In another mutant [*FoxJ1*$^{-/-}$(2), **C, F, I**] both sides are irregular and resemble control right epithelium, although sub-regions exhibit greater organization and polarity (arrowhead, **I**). In control (DMSO) frog embryos (**J, L, N**), left endoderm is more polarized than right, as indicated by enrichment of E-cadherin (Ecad; green) at apical adherens junctions (arrows, **L**), and concentration of apical polarity marker Par3 at the lumenal surface (red; arrowheads, **N**). In contrast, SB505124 (**K, M, O**) results in right isomerism, with left endoderm resembling right endoderm, as indicated by absence of apical enrichment of E-cadherin (**M**) and Par3 (**O**). left, L; right, R. Scalebars in **A-C**, 100 μM; **D-K**, 50 μM; **L-O**, 25 μM. (See also Fig. S4.)

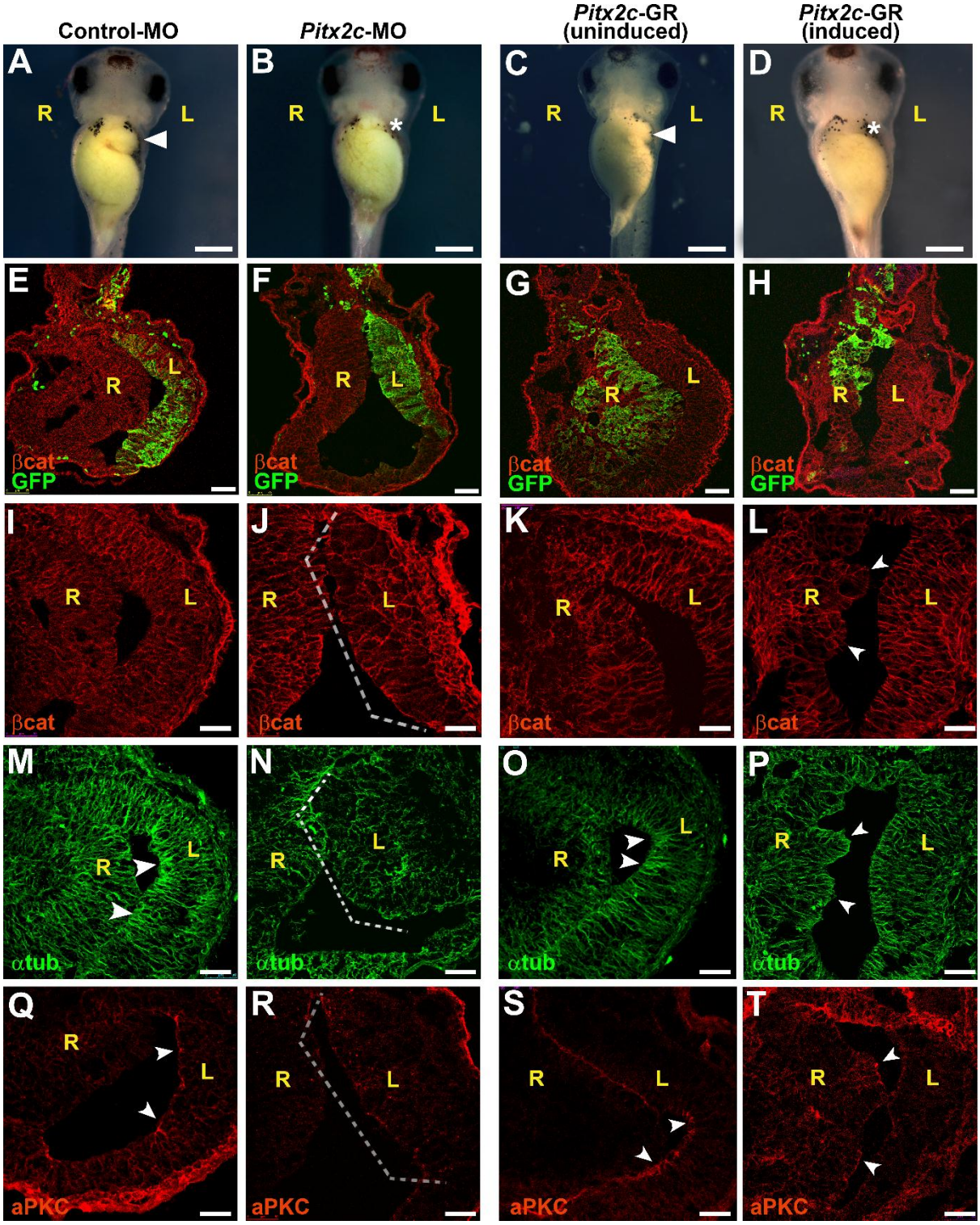

Figure 4. Pitx2c controls epithelial morphogenesis in left stomach wall. Frog embryos were injected with control-morpholino (Control-MO; **A, E, I, M, Q**) or *Pitx2c*-MO (**B, F, J, N, R**) targeted to the left side of the stomach, or injected with *Pitx2c*-GR mRNA (**C, G, K, O, S** and **D, H, L, P, T**) targeted to the right side. (See Fig. S6A-B for morpholino

validation.) In injected embryos (**A-D**), the greater curvature of the stomach at stage 42 is indicated by an arrowhead (**A, C**); absence of curvature is specified by an asterisk (**B, D**). Sections through stage 39 stomachs (**E-T**) were stained for β-catenin (βcat; red; **E-L**), α–tubulin (αtub; green; **M-P**), or atypical PKC (aPKC; red; **Q-T**). GFP mRNA was co-injected as a lineage tracer to confirm proper targeting (green; **E-H**). MO depletion on the left (**F**) or ectopic activity of Pitx2 on the right (**H**) results in a loss of asymmetry within the stomach compared to controls (**E** and **G**, respectively). In addition, compared to control-MO injected embryos, in which αtub and aPKC are concentrated at the apical surface of the left stomach wall (arrowheads in **M, Q**, respectively), MO depletion of Pitx2c disrupts epithelial architecture (brackets in **J, N, R**). Meanwhile, dexamethasone-induction of Pitx2c activity in the right wall polarizes stomach endoderm, as indicated by ectopic regions of polarized epithelial architecture (arrowheads in **L, P, T**), correlating with ectopic αtub (**P**) and aPKC (**T**), not observed in right wall of un-induced controls (**K, O, S**). Scalebars **A-D**, 500 μm; **E-H**, 75 μM; **I-T**, 50μM. left, L; right, R

Supplementary Information for

Stomach Curvature is Generated by Left-Right Asymmetric Gut Morphogenesis

Adam Davis, Nirav M. Amin, Caroline Johnson, Kristen Bagley, Troy Ghashghaei, Nanette Nascone-Yoder

Supplementary Materials and Methods

Mouse Genotyping

Phenol-choloroform-isoamyl alcohol extraction was used to obtain genomic DNA from embryonic yolk sacs. PCR primers used were:

GCE Forward – 5' CTC CCA CAT CAGGCA CAT GAG TAA 3'

GCE Reverse – 5' GCA AACAAC AGA TGG CTG GCA ACT 3'.

Xenopus Loss-of-function

The following morpholino sequences were used.

#1 (targets the *pitx2c* 5'UTR):	5'-ggtacagtacagtaggctcacagac-3'
#2 (targets the *pitx2c* ATG start site):	5'-gtaaagggtctttcatagagttcat-3'
Control (Genetools):	5'-cctcttacctcagttacaatttata-3'.

For CRISPR-Cas9 experiments, Tyrosinase gRNA was used as a positive control (Guo et al., 2014). *pitx2c* gRNA target sites were:

#1 GGAGTGTAAGTCAAGGCTAGAGG

#2 GGTGATGATGGTGGTGGTGATGG.

PCR primers used to amplify the *pitx2c* genomic locus targeted by gRNAs #1 and 2 were:

fwd 5'-GGCACCTGCCTTTAATGCTC- 3'

rev 5'-CACACCTGTGAGTAATCAGC- 3'.

Amplicons were denatured and allowed to slowly cool to allow formation of heteroduplex of wild-type and mutant products. Heteroduplexes were identified by digesting the product with T7 endonuclease I (NEB) as previously described (Guo et al., 2014). Uncut PCR products were subcloned into pCR2.1 vector (ThermoFisher Scientific) and individual clones were sequenced with M13R (5'-CAGGAAACAGCTATGAC-3') to determine mutation frequency. Sequencing was performed at the Eton Bioscience (Research Triangle Park, NC, USA).

Antibodies

Primary antibodies used for immunohistochemistry include anti-β-catenin (Santa Cruz, sc-7199, 1:100), anti-α-tubulin (Sigma, T9026, 1:1000), anti-aPKC (Santa Cruz, sc-216, 1:200), anti-integrin (Developmental Studies Hybridoma Bank, DSHB, , created by the NICHD of the NIH and maintained at The University of Iowa; 8C8, 1:1000), anti-γ-tubulin (Abcam, ab27074, 1:1000), anti-phospho-histone H3 (pHH3; Millipore, 06-570, 1;500), anti-E-cadherin (DSHB, 5D3-c, 1:200) and anti-Par3 (Millipore, 07-330, 1:200). Secondary antibodies used were Alexa 488-conjugated goat anti-mouse IgG (Invitrogen, A11029; 1:2000) and/or Alexa 546-conjugated goat anti-rabbit IgG (Invitrogen, A11035; 1:2000).

Antibodies used in Western blotting were rabbit anti-GFP (ThermoFisher, A6444, 1:1000), rabbit anti-GAPDH (Millipore, AB2302, 1:1000), and HRP-conjugated donkey anti-rabbit IgG (ThermoFisher, A16035, 1;10,000).

Methodology and Statistics

To ensure adequate power, at least 30 *Xenopus* embryos were used for each group/condition in each experiment. Mouse sample size was dependent on litter size from two independent breedings.

For *Xenopus* loss- and gain-of-function studies, embryos from a single clutch were randomly allocated to control or experimental groups; each experiment was performed at least 3 times, using independent breedings, with similar results.

For both mouse and *Xenopus* studies, results were validated by an independent researcher blinded to group allocation.

For mouse morphometric measurements, 2-3 sections were analyzed from at least 2 embryos. For *Xenopus* morphometric measurements, 2-3 sections were analyzed from at least 3 embryos.

For most analyses, a one-way Anova with post-hoc Tukey honest significant difference (HSD) was calculated, validated with additional Scheffé, Bonferroni and Holm multiple comparisons.

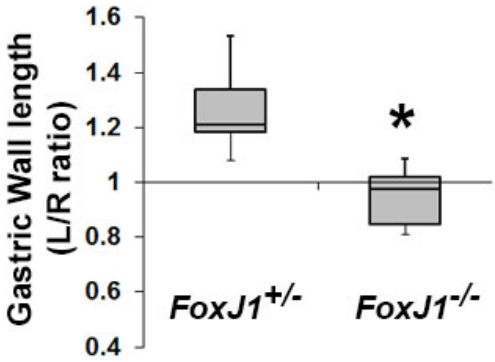

Figure S1. The normal left/right ratio of the lengths of the stomach walls is eliminated in E11.5 *FoxJ1*$^{-/-}$ mouse stomachs (* denotes p<0.01).

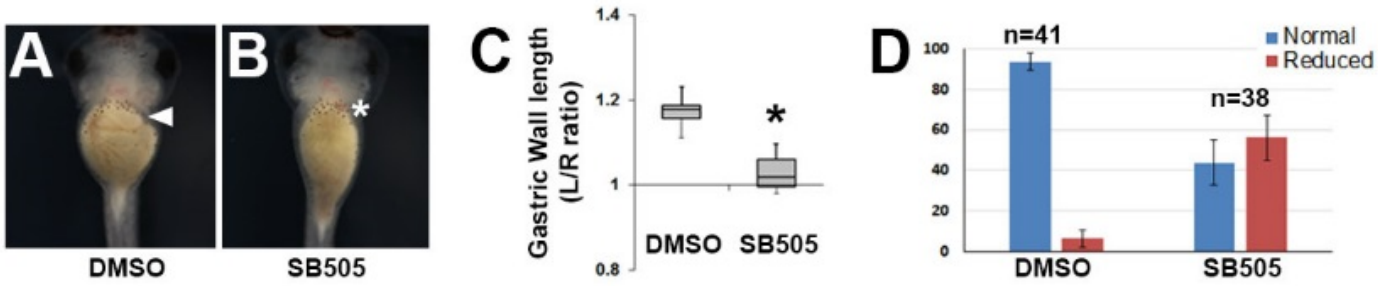

Figure S2. SB505124 exposure inhibits stomach curvature. Stage 19/20 frog embryos were exposed to DMSO (**A**) or 5μM SB505124 (**B**) through stage 42. **C**) The normal left/right (L/R) ratio of the lengths of the stomach walls is eliminated in SB505124-dosed embryos (* denotes $p<0.01$). The graph (**D**) indicates the percentage of embryos in which the greater curvature of the stomach is normal (e.g., arrowhead in **A**) or reduced/absent (* in **B**).

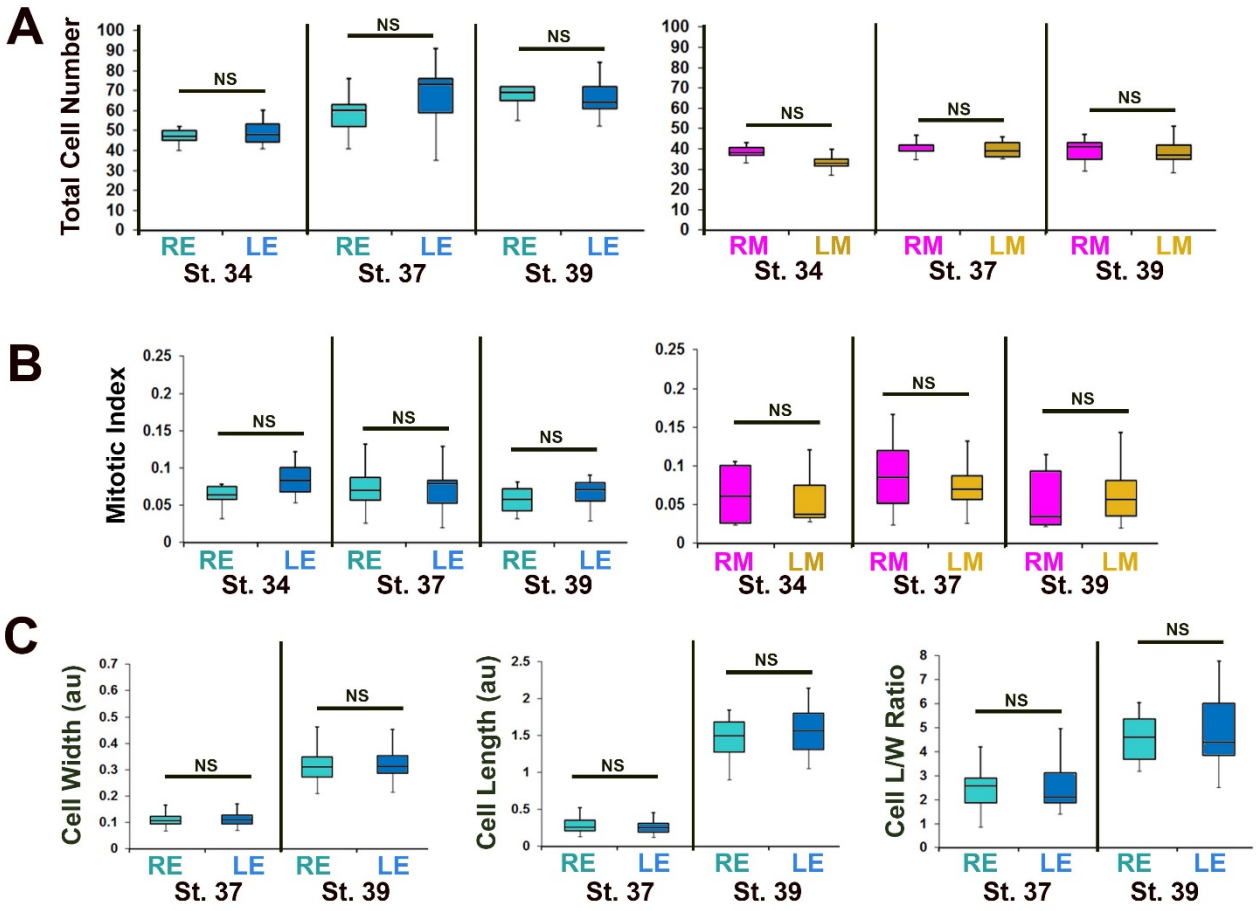

Figure S3. Morphometric comparison of cell properties in the left and right stomach walls. Sections of the developing stomach were immunohistochemically stained to reveal cell outlines or mitotic nuclei, and the indicated features were counted and/or measured at St. 34, 37 and 39, using at least 3 sections from each of 3 different embryos. At no stage are the total number of cells (**A**) or mitotic indices (**B**; number of pHH3+ cells/number of total cells) statistically different between the left and right sides. Likewise, there is no statistical difference in endoderm cell width, length or length/width (L/W) ratio between sides during curvature formation (**C**). RE, right endoderm; LE, left endoderm; RM, right mesoderm; LM, left mesoderm

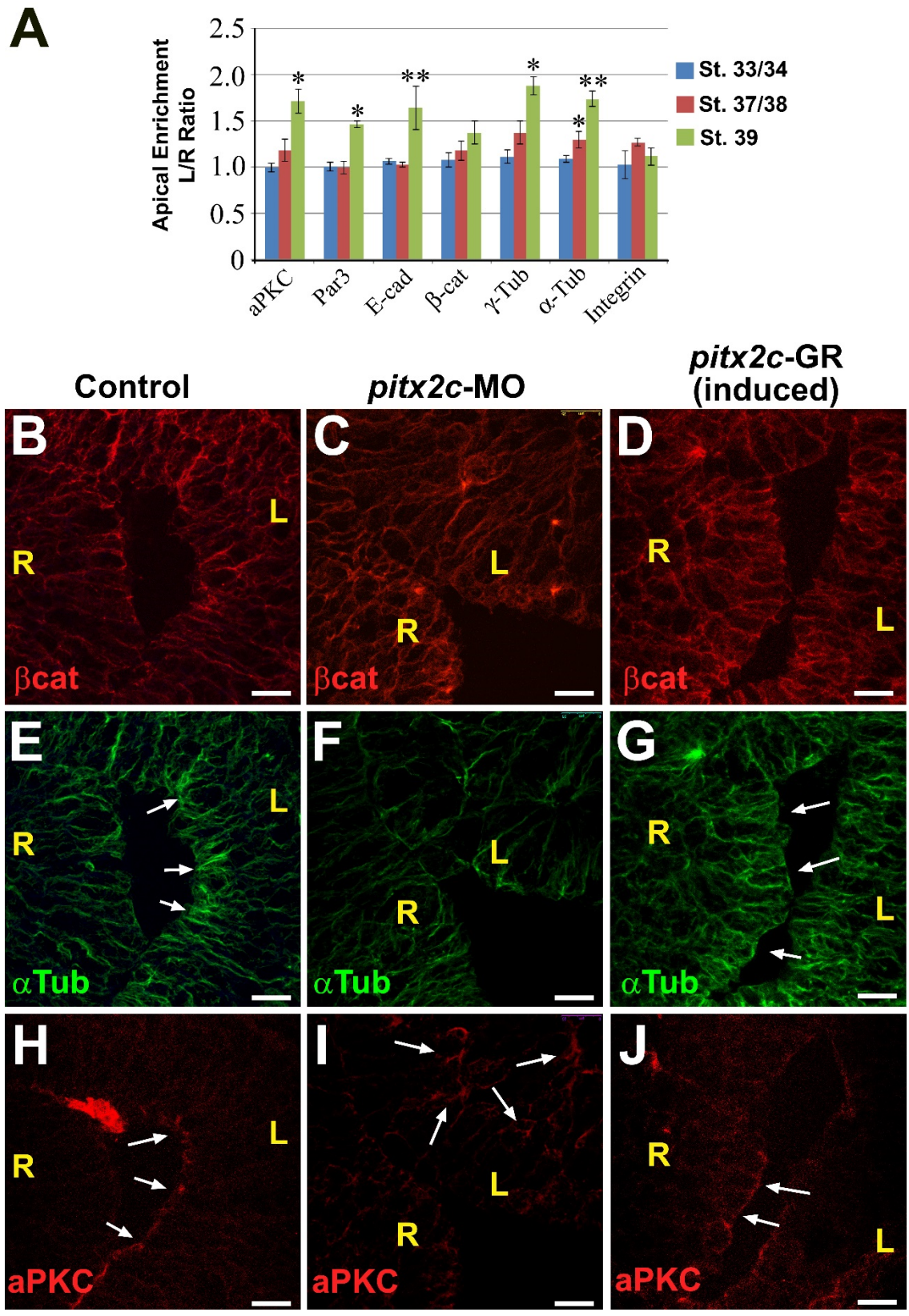

Figure S4. Markers of apicobasal polarity become left-right asymmetric in the developing stomach. The intensity of several markers of apical polarity, including aPKC, Par3, E-cadherin (E-cad), α-tubulin (α-tub) and γ-tubulin (γ-tub) were measured at the left and right surfaces of the frog stomach lumen at the indicated stages

using image J **(A)**. The level of apical enrichment is represented as a ratio of left and right intensities measured in at least 3 sections of 3-5 different embryos. The left/right (L/R) ratios of all apical markers become significantly different by stage 39, while the L/R ratios of β-catenin (β-cat) and integrin are not significantly >1. **B-J**) High magnification images of sections through the Stage 39 stomach stained for β-catenin (βcat; red; **B-D**), α−tubulin (αtub; green; **E-G**), or atypical PKC (aPKC; red; **H-J**). Compared to control embryos (**B, E, H**), in which αtub and aPKC are concentrated at the apical surface of the left stomach wall (arrowheads in **E, H,** respectively), MO depletion of Pitx2c (**C, F, I**) disrupts epithelial architecture (arrows in **I**). Meanwhile, dexamethasone-induction of Pitx2c activity (**D, G, J**) in the right wall ectopically polarizes the stomach endoderm, as indicated by ectopic regions of polarized epithelial architecture, correlating with enriched αtub and ectopic aPKC at the apical surface (arrows in **G, J**). Scalebars = 25uM. Left (L), Right (R).

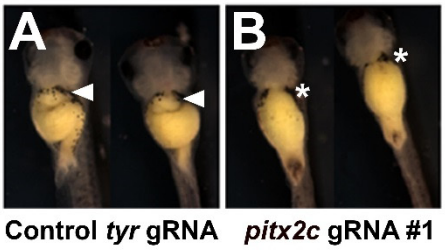

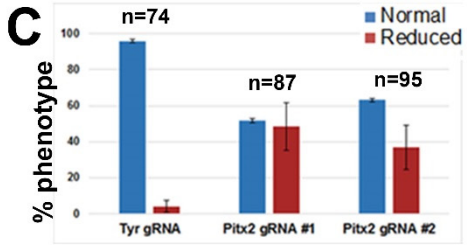

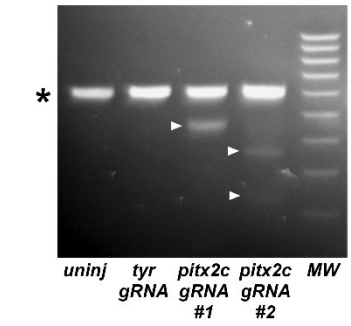

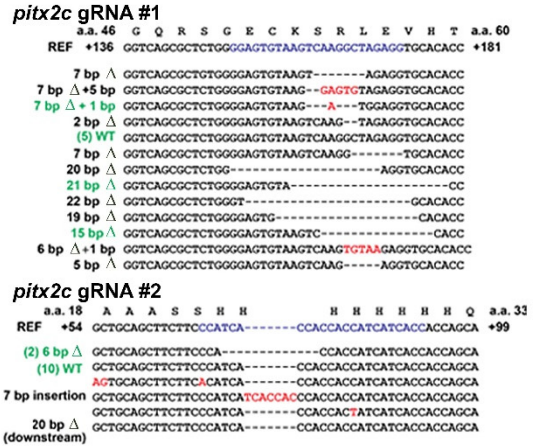

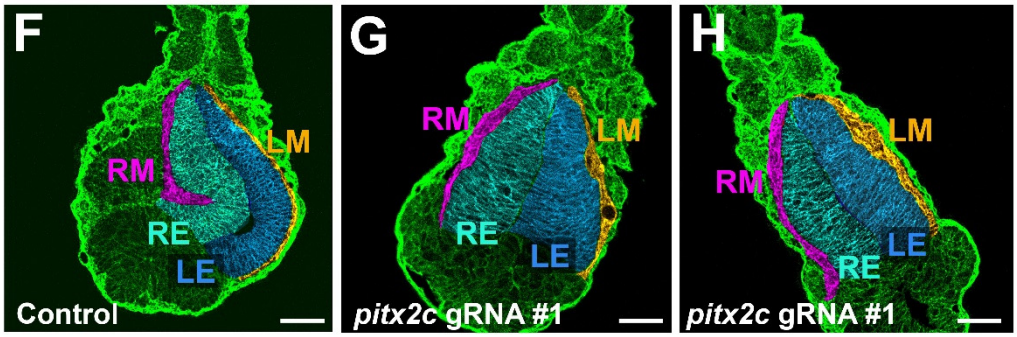

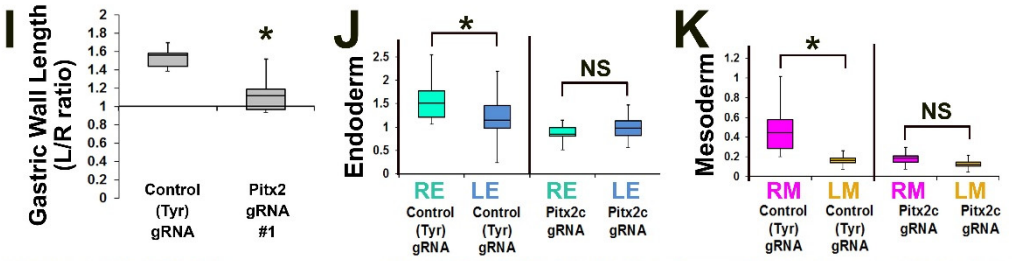

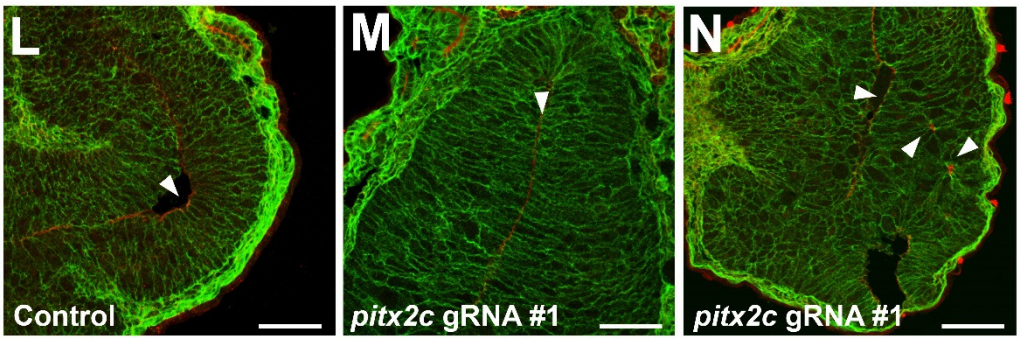

Figure S5. CRISPR-Cas9 mediated editing of *pitx2c* gene perturbs stomach asymmetry. *Xenopus* embryos were injected with 2 ng synthetic Cas9 mRNA plus 300 pg control *tyrosinase (tyr)* gRNA (**A**) or *pitx2c* gRNA (**B**), and allowed to develop until stage 42. The graph (**C**) indicates the percentage of embryos in which the greater curvature of the stomach is normal (arrowhead in **A**) or reduced/absent (* in **B**) after injection with the *tyr* gRNA or two different *pitx2*c gRNAs (#1 and #2). **D**) Genomic DNA from 10 embryos injected with each gRNA was pooled and PCR amplified using exon 1-specific primers, and then tested for CRISPR/Cas9-induced mutations by T7 endonuclease I assay. The asterisk (*) indicates the 500 bp amplicon not cut in un-injected or *tyr* gRNA-injected control embryos. Arrowheads indicate bands resulting from mismatches (inferred mutations) in amplicons cleaved by T7 endonuclease I. **E**) Sequencing of a subset of individual clones validates the presence of deleterious mutations in *pitx2c* gRNA injected embryos. For *pitx2c* gRNA #1, 9/17 mutations were likely nulls and 3/17 were predicted to result in compromised function; for *pitx2c* gRNA #2: 2/18 mutations were likely nulls and 4/17 were likely to result in compromised function. **F-N**) Sections through stomachs of Cas9 control and *pitx2c* gRNA (#1) injected embryos (Stage 39) were stained for integrin (green) and false color-coded as in Fig. 1 to highlight the relevant tissue layers (RE, right endoderm; LE, left endoderm; RM, right mesoderm; LM, left mesoderm). Controls show normal asymmetric expansion of the left stomach wall (**F**), but this is eliminated in embryos injected with *pitx2c* gRNA (**G-H**). Normal asymmetries in the lengths of the left and right stomach walls (**I**), and the widths of the endoderm (Endo) and mesoderm (Meso) layers (**J-K**), are also significantly perturbed by CRISPR-Cas editing of *pitx2c*; * denotes $p<0.01$. Compared to controls (**L**), left endoderm tissue architecture is severely disrupted, and apicobasal polarity is reduced (**M**), and/or disorganized (**N**) in embryos with CRISPR-mediated mutations in *pitx2c*; arrowheads indicate the expression of the apical marker aPKC (red). Scalebars= 100 μM.

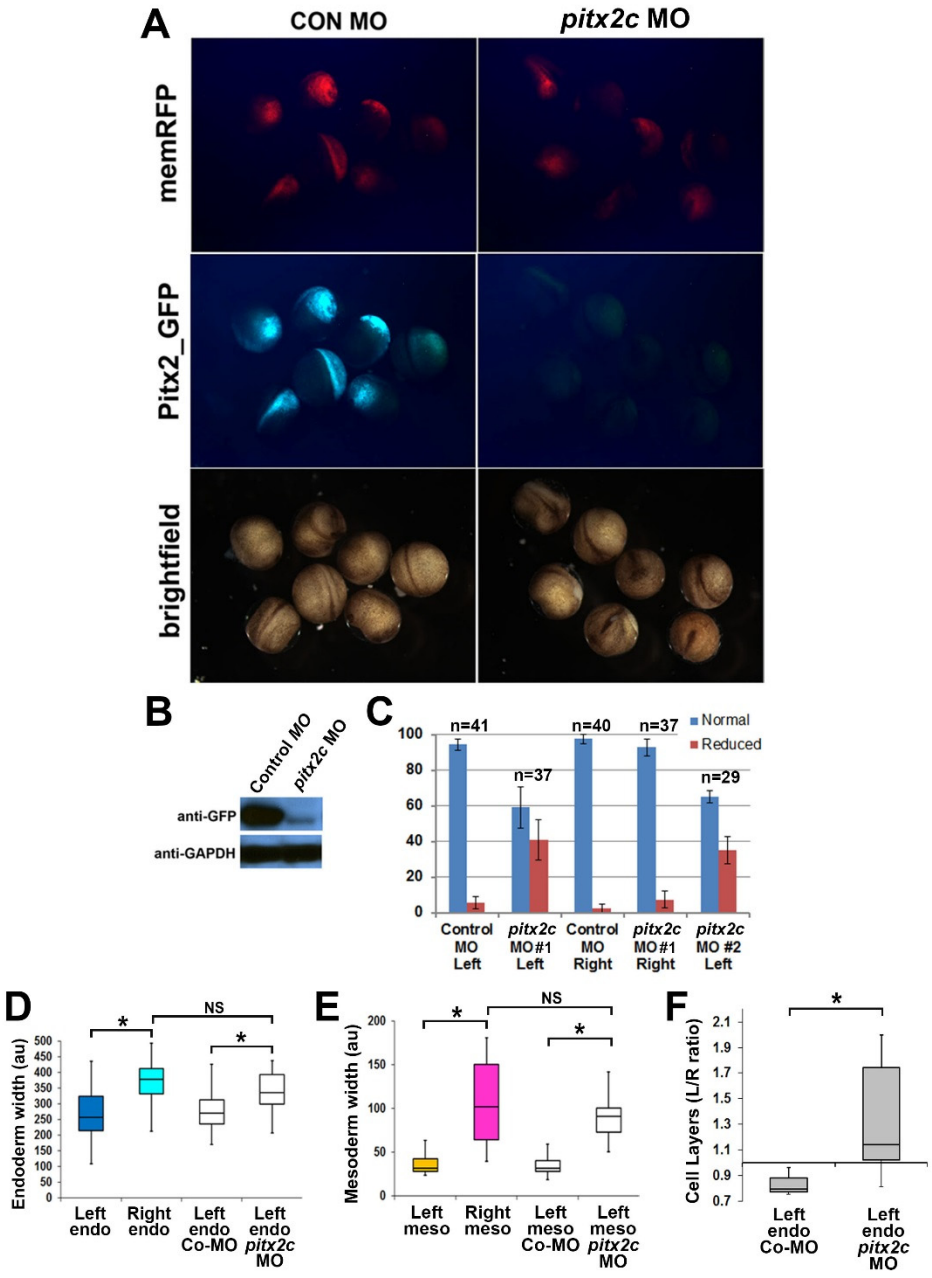

Figure S6. Specificity and efficacy of the *pitx2c* MO. A) *Xenopus* embryos (8-cell stage) were injected with 8 ng Control or *pitx2c* MO plus 200pg RFP mRNA and GFP mRNA (fused with *pitx2c* 5' UTR MO target site), and cultured until stage 20. Effective translation, indicated by GFP fluorescence, is visible in embryos injected with Control MO, but not with *Pitx2c* MO; RFP (which does not contain the *pitx2c* 5' UTR sequence) levels remain unaffected. **B**) Western blot confirms drastic reduction of GFP protein levels in embryonic extracts from *pitx2c*-MO- but not Control-MO-injected embryos. GAPDH, loading control. **C**) The graph indicates the frequency (percentage) of embryos in which the greater curvature of the stomach is normal or reduced/absent when Control MO or *pitx2c*-MO (#1) is targeted to either the left or right side. A second, independent MO (*pitx2c* MO #2) confirmed the result. While injection of Control MO has no effect on the relative thickness of the left endoderm (**D**) or mesoderm (**E**), *pitx2c*-MO-injected tissues are similar in thickness to the normal (non-*pitx2c*-expressing) right tissues (i.e., not significantly different, NS). **F**) The L/R ratio of endoderm cell layers is significantly increased in *pitx2c*-MO-injected stomachs, compared to Control-MO. * denotes $p<0.01$

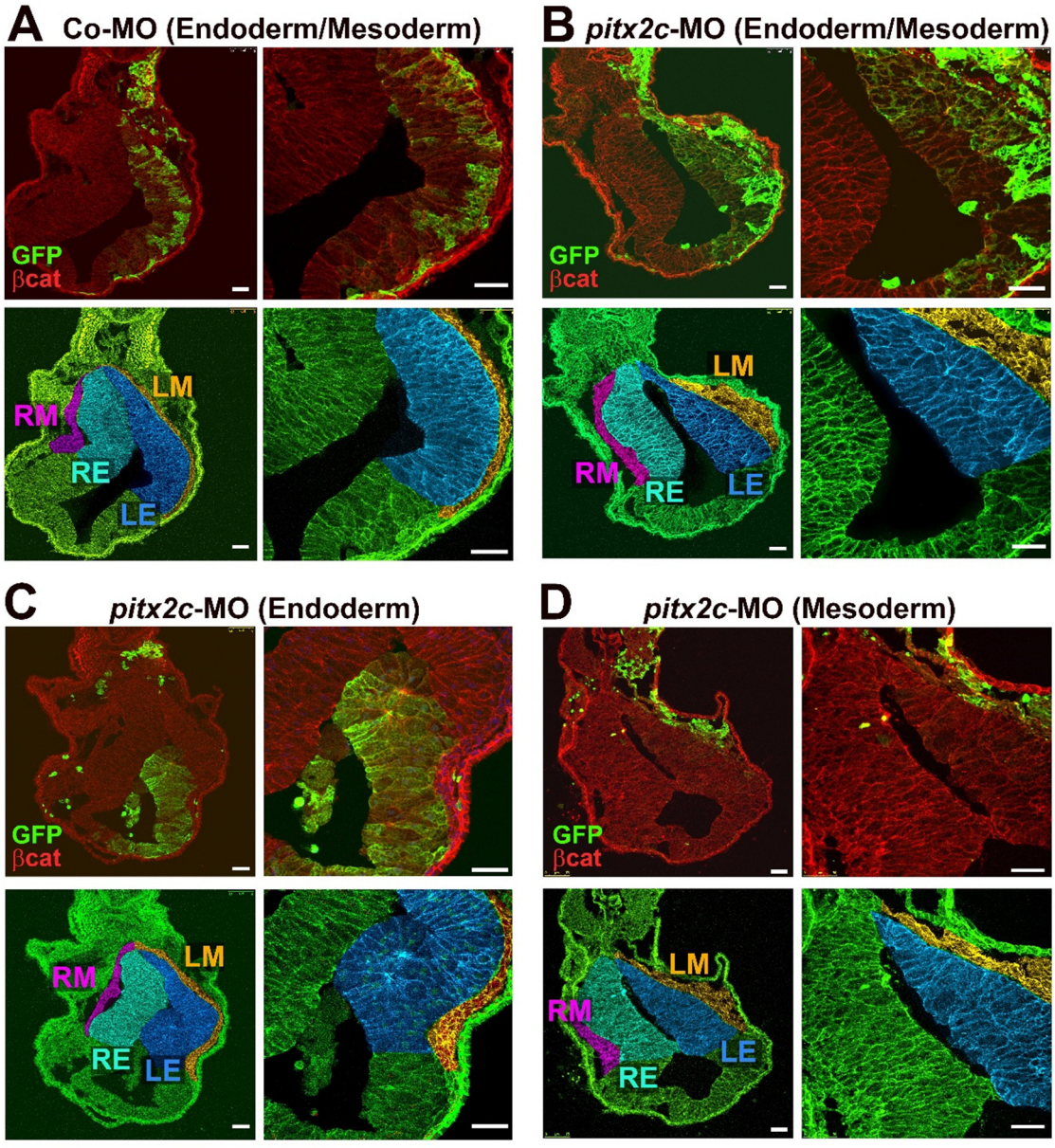

Figure S7. Reciprocal endoderm-mesoderm interactions affect morphogenesis of the left stomach wall. Frog embryos were injected with GFP mRNA and either control morpholino (Co-MO; **A**) or *pitx2c*-MO (**B-D**), targeted to the left side of the stomach. Top panels: sections through the stomach were stained for β-catenin (βcat; red) and GFP (green). Bottom panels: the same sections were false color-coded as in Fig. 1(b) to highlight the relevant tissue layers (RE, right endoderm; LE, left endoderm; RM, right mesoderm; LM, left mesoderm). In the embryo shown in **A**, Control-MO is distributed throughout the LE and LM of the left stomach wall, which exhibits normal left side tissue architecture. In the embryo shown in **B**, *pitx2c*-MO is distributed throughout the LE and LM, and both tissue layers are abnormally thickened and/or disorganized. In **C**, *pitx2c*-MO is present predominately in the LE, with minimal contribution to the LM; yet, both the LE and LM are abnormal. Likewise, in **D**, *pitx2c*-MO is present only in the LM, with minimal contribution to LE, but both LE and LM are abnormal.

Supplementary Information for

Stomach Curvature is Generated by Left-Right Asymmetric Gut Morphogenesis

Adam Davis, Nirav M. Amin, Caroline Johnson, Kristen Bagley, Troy Ghashghaei, Nanette Nascone-Yoder

Supplementary Materials and Methods

Mouse Genotyping

Phenol-choloroform-isoamyl alcohol extraction was used to obtain genomic DNA from embryonic yolk sacs. PCR primers used were:

GCE Forward – 5' CTC CCA CAT CAGGCA CAT GAG TAA 3'

GCE Reverse – 5' GCA AACAAC AGA TGG CTG GCA ACT 3'.

Xenopus Loss-of-function

The following morpholino sequences were used.

#1 (targets the *pitx2c* 5'UTR):	5'-ggtacagtacagtaggctcacagac-3'
#2 (targets the *pitx2c* ATG start site):	5'-gtaaagggtctttcatagagttcat-3'
Control (Genetools):	5'-cctcttacctcagttacaatttata-3'.

For CRISPR-Cas9 experiments, Tyrosinase gRNA was used as a positive control (Guo et al., 2014). *pitx2c* gRNA target sites were:

#1 GGAGTGTAAGTCAAGGCTAGAGG

#2 GGTGATGATGGTGGTGGTGATGG.

PCR primers used to amplify the *pitx2c* genomic locus targeted by gRNAs #1 and 2 were:

fwd 5'-GGCACCTGCCTTTAATGCTC- 3'

rev 5'-CACACCTGTGAGTAATCAGC- 3'.

Amplicons were denatured and allowed to slowly cool to allow formation of heteroduplex of wild-type and mutant products. Heteroduplexes were identified by digesting the product with T7 endonuclease I (NEB) as previously described (Guo et al., 2014). Uncut PCR products were subcloned into pCR2.1 vector (ThermoFisher Scientific) and individual clones were sequenced with M13R (5'-CAGGAAACAGCTATGAC-3') to determine mutation frequency. Sequencing was performed at the Eton Bioscience (Research Triangle Park, NC, USA).

Antibodies

Primary antibodies used for immunohistochemistry include anti-β-catenin (Santa Cruz, sc-7199, 1:100), anti-α-tubulin (Sigma, T9026, 1:1000), anti-aPKC (Santa Cruz, sc-216, 1:200), anti-integrin (Developmental Studies Hybridoma Bank, DSHB, , created by the NICHD of the NIH and maintained at The University of Iowa; 8C8, 1:1000), anti-γ-tubulin (Abcam, ab27074, 1:1000), anti-phospho-histone H3 (pHH3; Millipore, 06-570, 1;500), anti-E-cadherin (DSHB, 5D3-c, 1:200) and anti-Par3 (Millipore, 07-330, 1:200). Secondary antibodies used were Alexa 488-conjugated goat anti-mouse IgG (Invitrogen, A11029; 1:2000) and/or Alexa 546-conjugated goat anti-rabbit IgG (Invitrogen, A11035; 1:2000). Nuclear staining was accomplished with TO-PRO-3 Iodide (T3605; 1:1000).

Antibodies used in Western blotting were rabbit anti-GFP (ThermoFisher, A6455, 1:1000), rabbit anti-GAPDH (Millipore, AB2302, 1:1000), and HRP-conjugated donkey anti-rabbit IgG (ThermoFisher, A16035, 1;10,000).

Methodology and Statistics

To ensure adequate power, at least 30 *Xenopus* embryos were used for each group/condition in each experiment. Mouse sample size was dependent on litter size from two independent breedings.

For *Xenopus* loss- and gain-of-function studies, embryos from a single clutch were randomly allocated to control or experimental groups; each experiment was performed at least 3 times, using independent breedings, with similar results.

For both mouse and *Xenopus* studies, results were validated by an independent researcher blinded to group allocation.

For mouse morphometric measurements, 2-3 sections were analyzed from at least 2 embryos. For *Xenopus* morphometric measurements, 2-3 sections were analyzed from at least 3 embryos.

For most analyses, a one-way Anova with post-hoc Tukey honest significant difference (HSD) was calculated, validated with additional Scheffé, Bonferroni and Holm multiple comparisons.

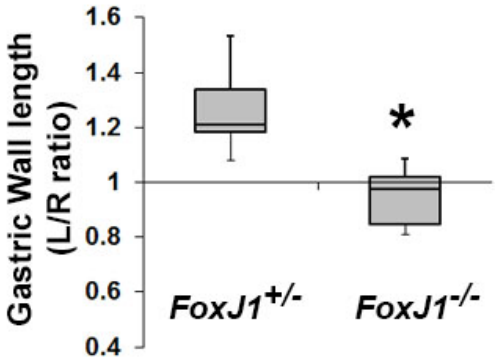

Figure S1. The normal left/right ratio of the lengths of the stomach walls is eliminated in E11.5 *FoxJ1*$^{-/-}$ mouse stomachs (* denotes p<0.01).

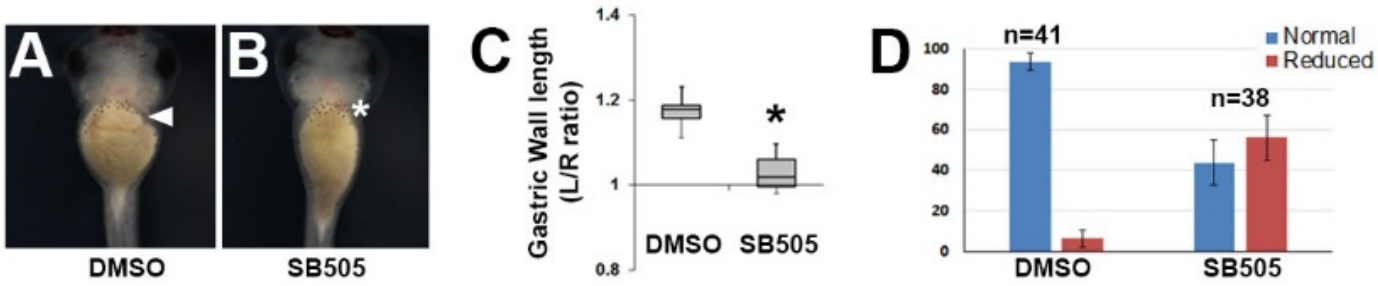

Figure S2. SB505124 exposure inhibits stomach curvature. Stage 19/20 frog embryos were exposed to DMSO (**A**) or 5μM SB505124 (**B**) through stage 42. **C**) The normal left/right (L/R) ratio of the lengths of the stomach walls is eliminated in SB505124-dosed embryos (* denotes $p<0.01$). The graph (**D**) indicates the percentage of embryos in which the greater curvature of the stomach is normal (e.g., arrowhead in **A**) or reduced/absent (* in **B**).

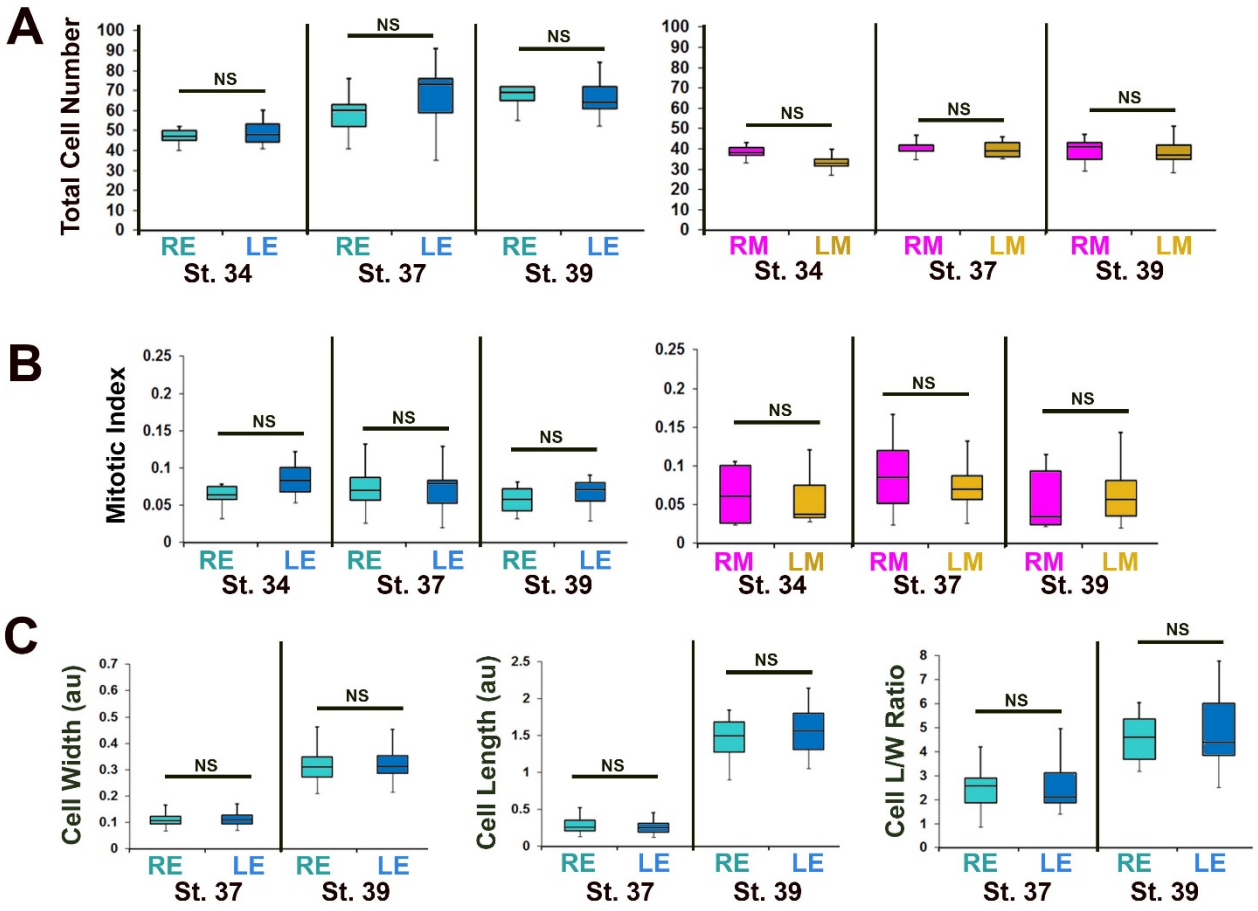

Figure S3. Morphometric comparison of cell properties in the left and right stomach walls. Sections of the developing stomach were immunohistochemically stained to reveal cell outlines or mitotic nuclei, and the indicated features were counted and/or measured at St. 34, 37 and 39, using at least 3 sections from each of 3 different embryos. At no stage are the total number of cells (**A**) or mitotic indices (**B**; number of pHH3+ cells/number of total cells) statistically different between the left and right sides. Likewise, there is no statistical difference in endoderm cell width, length or length/width (L/W) ratio between sides during curvature formation (**C**). RE, right endoderm; LE, left endoderm; RM, right mesoderm; LM, left mesoderm

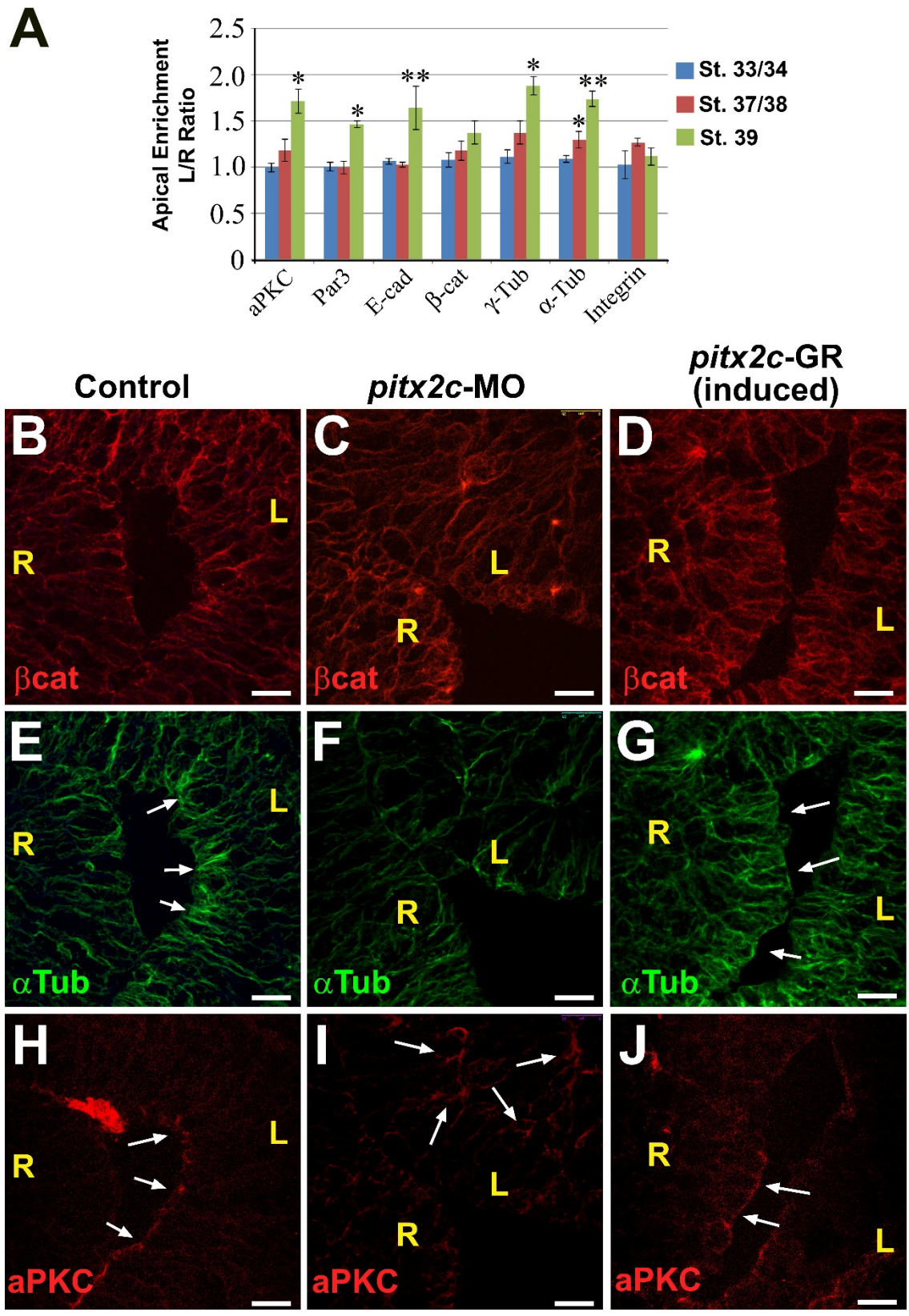

Figure S4. Markers of apicobasal polarity become left-right asymmetric in the developing stomach. The intensity of several markers of apical polarity, including aPKC, Par3, E-cadherin (E-cad), α-tubulin (α-tub) and γ-tubulin (γ-tub) were measured at the left and right surfaces of the frog stomach lumen at the indicated stages

using image J **(A)**. The level of apical enrichment is represented as a ratio of left and right intensities measured in at least 3 sections of 3-5 different embryos. The left/right (L/R) ratios of all apical markers become significantly different by stage 39, while the L/R ratios of β-catenin (β-cat) and integrin are not significantly >1. **B-J**) High magnification images of sections through the Stage 39 stomach stained for β-catenin (βcat; red; **B-D**), α−tubulin (αtub; green; **E-G**), or atypical PKC (aPKC; red; **H-J**). Compared to control embryos (**B, E, H**), in which αtub and aPKC are concentrated at the apical surface of the left stomach wall (arrowheads in **E, H,** respectively), MO depletion of Pitx2c (**C, F, I**) disrupts epithelial architecture (arrows in **I**). Meanwhile, dexamethasone-induction of Pitx2c activity (**D, G, J**) in the right wall ectopically polarizes the stomach endoderm, as indicated by ectopic regions of polarized epithelial architecture, correlating with enriched αtub and ectopic aPKC at the apical surface (arrows in **G, J**). Scalebars = 25uM. Left (L), Right (R).

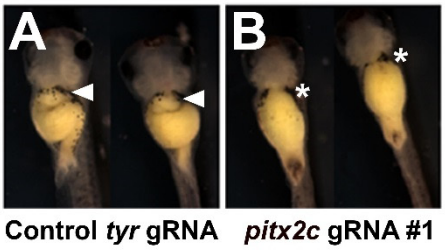

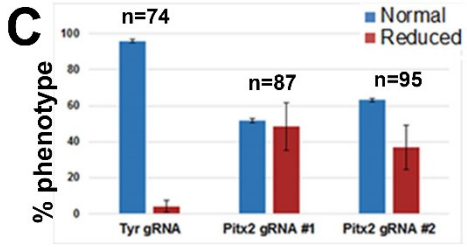

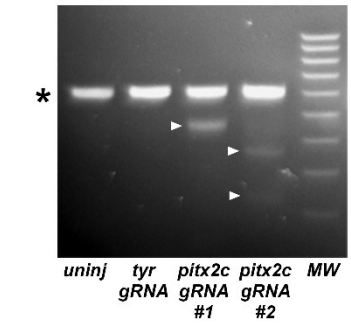

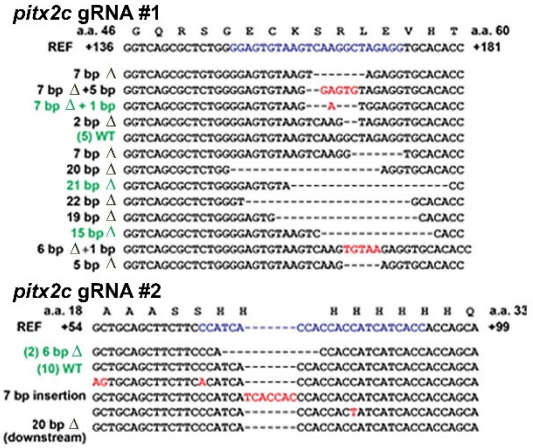

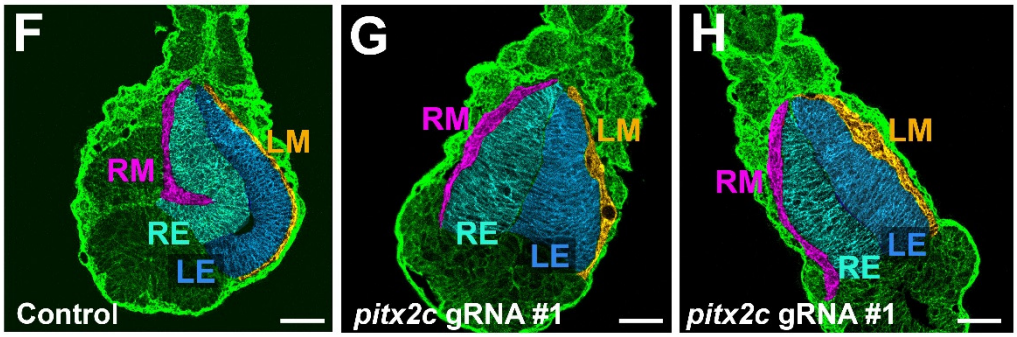

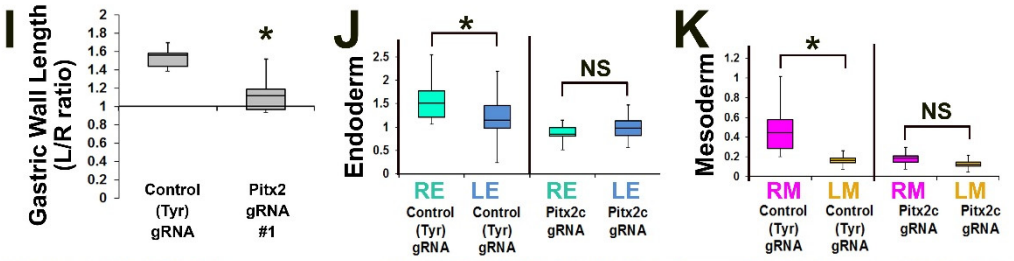

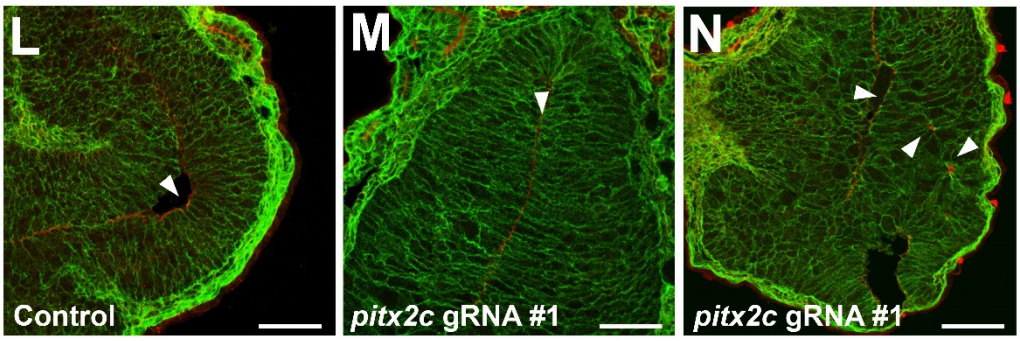

Figure S5. CRISPR-Cas9 mediated editing of *pitx2c* gene perturbs stomach asymmetry. *Xenopus* embryos were injected with 2 ng synthetic Cas9 mRNA plus 300 pg control *tyrosinase (tyr)* gRNA (**A**) or *pitx2c* gRNA (**B**), and allowed to develop until stage 42. The graph (**C**) indicates the percentage of embryos in which the greater curvature of the stomach is normal (arrowhead in **A**) or reduced/absent (* in **B**) after injection with the *tyr* gRNA or two different *pitx2*c gRNAs (#1 and #2). **D**) Genomic DNA from 10 embryos injected with each gRNA was pooled and PCR amplified using exon 1-specific primers, and then tested for CRISPR/Cas9-induced mutations by T7 endonuclease I assay. The asterisk (*) indicates the 500 bp amplicon not cut in un-injected or *tyr* gRNA-injected control embryos. Arrowheads indicate bands resulting from mismatches (inferred mutations) in amplicons cleaved by T7 endonuclease I. **E**) Sequencing of a subset of individual clones validates the presence of deleterious mutations in *pitx2c* gRNA injected embryos. For *pitx2c* gRNA #1, 9/17 mutations were likely nulls and 3/17 were predicted to result in compromised function; for *pitx2c* gRNA #2: 2/18 mutations were likely nulls and 4/17 were likely to result in compromised function. **F-N**) Sections through stomachs of Cas9 control and *pitx2c* gRNA (#1) injected embryos (Stage 39) were stained for integrin (green) and false color-coded as in Fig. 1 to highlight the relevant tissue layers (RE, right endoderm; LE, left endoderm; RM, right mesoderm; LM, left mesoderm). Controls show normal asymmetric expansion of the left stomach wall (**F**), but this is eliminated in embryos injected with *pitx2c* gRNA (**G-H**). Normal asymmetries in the lengths of the left and right stomach walls (**I**), and the widths of the endoderm (Endo) and mesoderm (Meso) layers (**J-K**), are also significantly perturbed by CRISPR-Cas editing of *pitx2c*; * denotes $p<0.01$. Compared to controls (**L**), left endoderm tissue architecture is severely disrupted, and apicobasal polarity is reduced (**M**), and/or disorganized (**N**) in embryos with CRISPR-mediated mutations in *pitx2c*; arrowheads indicate the expression of the apical marker aPKC (red). Scalebars= 100 μM.

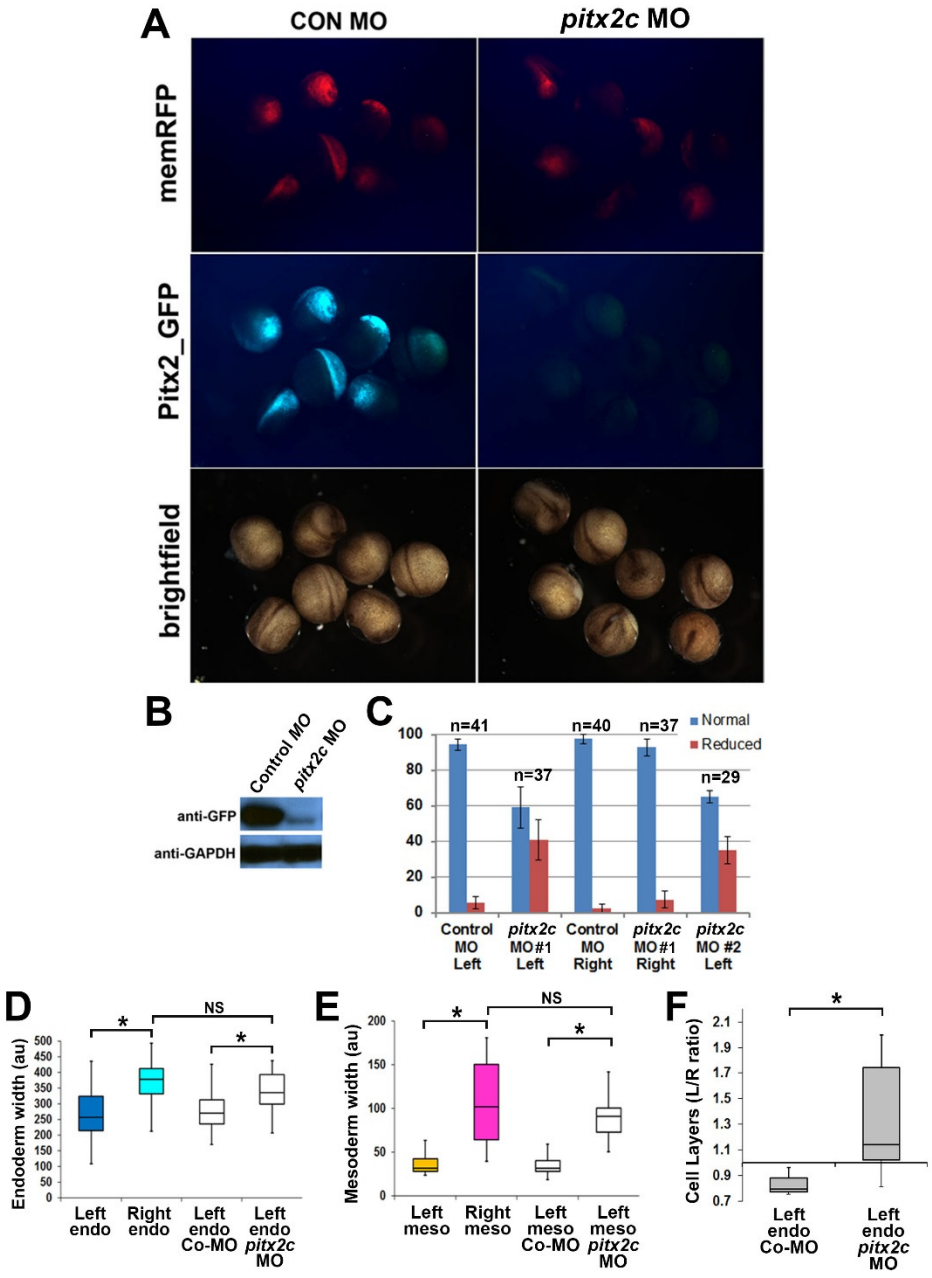

Figure S6. Specificity and efficacy of the *pitx2c* MO. A) *Xenopus* embryos (8-cell stage) were injected with 8 ng Control or *pitx2c* MO plus 200pg RFP mRNA and GFP mRNA (fused with *pitx2c* 5' UTR MO target site), and cultured until stage 20. Effective translation, indicated by GFP fluorescence, is visible in embryos injected with Control MO, but not with *Pitx2c* MO; RFP (which does not contain the *pitx2c* 5' UTR sequence) levels remain unaffected. **B**) Western blot confirms drastic reduction of GFP protein levels in embryonic extracts from *pitx2c*-MO- but not Control-MO-injected embryos. GAPDH, loading control. **C**) The graph indicates the frequency (percentage) of embryos in which the greater curvature of the stomach is normal or reduced/absent when Control MO or *pitx2c*-MO (#1) is targeted to either the left or right side. A second, independent MO (*pitx2c* MO #2) confirmed the result. While injection of Control MO has no effect on the relative thickness of the left endoderm (**D**) or mesoderm (**E**), *pitx2c*-MO-injected tissues are similar in thickness to the normal (non-*pitx2c*-expressing) right tissues (i.e., not significantly different, NS). **F**) The L/R ratio of endoderm cell layers is significantly increased in *pitx2c*-MO-injected stomachs, compared to Control-MO. * denotes $p<0.01$

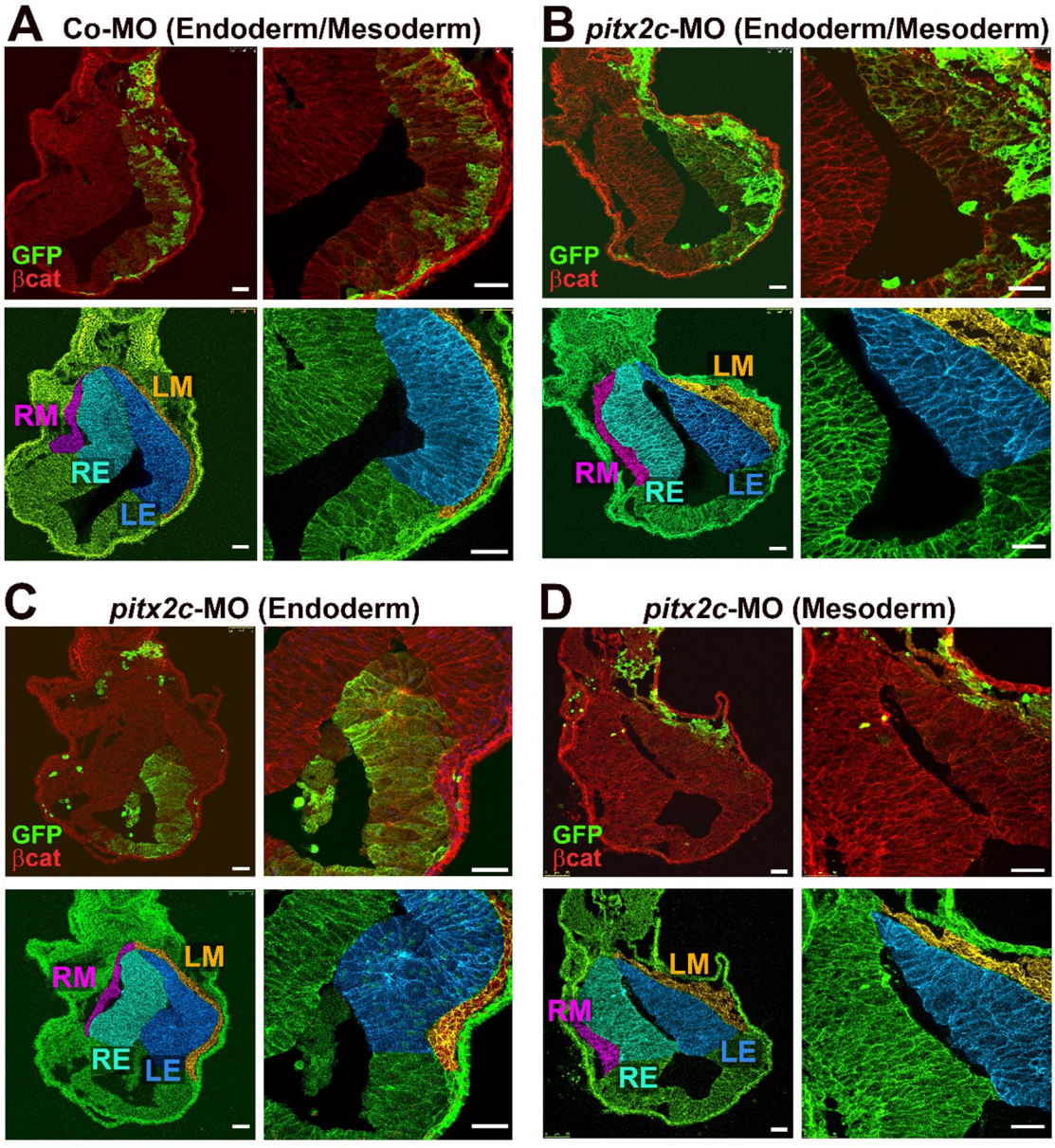

Figure S7. Reciprocal endoderm-mesoderm interactions affect morphogenesis of the left stomach wall. Frog embryos were injected with GFP mRNA and either control morpholino (Co-MO; **A**) or *pitx2c*-MO (**B-D**), targeted to the left side of the stomach. Top panels: sections through the stomach were stained for β-catenin (βcat; red) and GFP (green). Bottom panels: the same sections were false color-coded as in Fig. 1(b) to highlight the relevant tissue layers (RE, right endoderm; LE, left endoderm; RM, right mesoderm; LM, left mesoderm). In the embryo shown in **A**, Control-MO is distributed throughout the LE and LM of the left stomach wall, which exhibits normal left side tissue architecture. In the embryo shown in **B**, *pitx2c*-MO is distributed throughout the LE and LM, and both tissue layers are abnormally thickened and/or disorganized. In **C**, *pitx2c*-MO is present predominately in the LE, with minimal contribution to the LM; yet, both the LE and LM are abnormal. Likewise, in **D**, *pitx2c*-MO is present only in the LM, with minimal contribution to LE, but both LE and LM are abnormal.